THESIS FOR THE DEGREE OF DOCTOR OF PHILOSOPHY

Melt-processing and properties of thermoplastic composites based on ethylene-acrylic acid copolymer reinforced with wood nanocellulose

ABHIJIT VENKATESH

Department of Industrial and Materials Science

CHALMERS UNIVERSITY OF TECHNOLOGY
Gothenburg, Sweden 2020

Melt-processing and properties of thermoplastic composites based on ethylene-acrylic acid copolymer reinforced with wood nanocellulose
ABHIJIT VENKATESH
ISBN 978-91-7905-421-2

Doktorsavhandlingar vid Chalmers tekniska högskola
Ny serie nr 4888
ISSN 0346-718X

Department of Industrial and Materials Science
Chalmers University of Technology
SE-412 96 Gothenburg
Sweden
Telephone + 46 (0)31-772 1000

Cover:
[Prototype beverage carton caps and straws reinforced with nanocellulose]

Chalmers Reproservice
Gothenburg, Sweden 2020

To Appa and Amma

Melt-processing and properties of thermoplastic composites based on ethylene-acrylic acid copolymer reinforced with wood nanocellulose

Abhijit Venkatesh

Department of Industrial and Materials Science
Chalmers University of Technology

ABSTRACT

Composites reinforced with cellulose nanofibers (CNF), both modified and unmodified cellulose nanocrystals (CNC) and pulp fibers have been prepared through small-scale and large-scale methods. The composites were produced by water-assisted dispersion mixing, drying and compression moulding on the laboratory scale and by extrusion and injection moulding for the large-scale production. The compression-moulded composites were stiffer and stronger by a factor of more than 10 for the CNF or pulp-based samples (>50 wt%) and by a factor of 3 for the CNC-based composites (at 10 wt%). The addition of a lubricant to pulp-based fibers resulted in a behaviour similar to that of a compatibilizer at low concentrations and to that of both compatibilizer and lubricant at higher concentrations.

However, when the processing was scaled up, the improvement in properties was much less for the CNF-based and CNC-based composites after being melt-processed via extrusion and injection moulding, despite the fact that they showed a percolated cellulose network. Although the scale-up was successful, aggregates were observed. These aggregates could be reduced to some extent by changing the process design and parameters. Water-assisted extrusion was also used to reduce the aggregation but there was little improvement in properties. It is suggested that the extent of melt flow in the processing method influences the final properties of the composites, despite the nanoscale reinforcement.

Keywords: *Cellulose, Cellulose nanofibers, Cellulose nanocrystals, Composite, Melt rheology, Mechanical properties, Extrusion, Injection moulding, Pulp fibers*

LIST OF PUBLICATIONS

The thesis is based on the following papers, referred to by Roman numerals in the text. The work was performed at the Department of Industrial and Materials Science at Chalmers University of Technology between February 2016 and January 2021 under the supervision of Professor Antal Boldizar.

List of appended papers:

I **Cellulose nanofibril-reinforced composites using aqueous dispersed ethylene-acrylic acid copolymer**
Venkatesh A, Thunberg J, Moberg T, Klingberg M, Hammar L, Peterson A, Müller C & Boldizar A
(2018) *Cellulose*, 25(8) p. 4577-4589
Reprinted with permission from Springer

II **Composites with surface-grafted cellulose nanocrystals (CNC)**
L. Forsgren, K. Sahlin-Sjövold, A. Venkatesh, J. Thunberg, R. Kádár, A. Boldizar, G. Westman & M. Rigdahl
(2019) *Journal of Materials Science*, 54(4) p.3009-3022
Reprinted with permission from Springer

III **Melt processing of ethylene-acrylic acid copolymer composites reinforced with nanocellulose**
Venkatesh A, Thunberg J, K. Sahlin-Sjövold, M. Rigdahl & A. Boldizar
(2020) *Polymer Engineering and Science*, 60(5) p.956-967
Reprinted with permission from Wiley

IV **Molybdenum disulphide – A traditional external lubricant that shows interesting interphase improvements in pulp based biocomposites**
Ehsan Hosseini, A. Venkatesh, A. Boldizar & G. Westman
Submitted for publication

V **Water-assisted extrusion and injection moulding of composites with surface-grafted cellulose nanocrystals – an upscaling study**
L. Forsgren, A. Venkatesh, F. Rigoulet, K. Sahlin-Sjövold, G. Westman, M. Rigdahl & A. Boldizar
Submitted for publication

Papers not included in the thesis

VI **Water-assisted melt-processing of beverage carton caps made of polycaprolactone or poly(ethylene-acrylic acid) reinforced with wood-nanocellulose**
A. Venkatesh, L. Forsgren, A. Avella, F. Vilaseca, G. Lo Re & A. Boldizar
Manuscript, to be submitted

VII **Water-assisted extrusion of polycaprolactone reinforced with thermomechanical pulp**
A. Venkatesh, A. Avella, L. Forsgren, G. Lo Re & A. Boldizar
Manuscript, to be submitted

VIII **Dynamic nanocellulose networks for thermoset-like yet recyclable plastics with a high melt stiffness and creep resistance**
Peterson A, Östergren I, Lotsari A, Venkatesh A, Thunberg J, Ström A, Rojas R, Andersson M, Berglund L.A, Boldizar A, Müller C
(2019) *Biomacromolecules*, 20(10) p.3924-3932

IX **Plasticizing starch by adding magnesium chloride or sodium chloride**
A. Venkatesh & A. Boldizar
(2017) *Starch/Staerke*, 68(5-6) p.1-9

CONTRIBUTION REPORT

The author's contribution to the papers presented in the thesis:

Paper I — Main author. Planned and performed all the experiments and characterization together with Johannes Thunberg. The CT-scan data was analysed with the help of Lars Hammar and the rheology of the suspensions was studied together with Tobias Moberg and Maria Klinberg. The author wrote the manuscript together with Johannes Thunberg, with input from the other co-authors.

Paper II — Third author. The author was involved in the planning and performed sample preparation, tensile testing and thermal analysis. The author planned and performed the DMA measurements. The CNC preparation was mainly done by Karin Sahlin-Sjövold and Lilian Forsgren. The author contributed to the manuscript preparation together with Lilian and Karin Sahlin-Sjövold.

Paper III — Main author. The author planned and performed all the experiments and characterization except for zeta-potential measurements which was performed by Karin Sahlin-Sjövold. The author wrote the manuscript together with Johannes Thunberg and with the input of the other co-authors.

Paper IV — Shared main author. The author planned and performed sample preparation, mechanical testing, DMA and sample preparation for scanning electron microscopy. The thermal analysis, FTIR, EDX and SEM studies were mainly performed by Ehsan Hosseini. The author wrote the manuscript together with Ehsan Hosseini with input from the other co-authors.

Paper V — Second author. The author planned and performed all the experiments and characterization together with Lilian Forsgren. The CNC preparation was mainly done by and Lilian Forsgren and Karin Sahlin-Sjövold. The author wrote the manuscript together with Lilian Forsgren and with input from the other co-authors.

ABBREVIATIONS

AA – Acrylic acid

AFM – Atomic force Microscopy

ATR – Attenuated total reflectance

CNC – Cellulose nanocrystals

CNF – Cellulose nanofibers

DMA – Dynamic mechanical analysis

DP – Dissolving pulp

DSC – Differential scanning calorimetry

E - Ethylene

EAA – Ethylene-acrylic acid copolymer

EDX – Energy dispersive X-ray spectroscopy

FTIR – Fourier transform infrared spectroscopy

IM – Injection moulding

LDPE – Low-density polyethylene

MCC – Micro-crystalline cellulose

NMR – Nuclear magnetic resonance

SEM – Scanning electron microscopy

SSE – Single screw extruder

TGA – Thermo-gravimetric analysis

TMP – Thermomechanical pulp

TSE – Twin-screw extruder

TABLE OF CONTENTS

1 INTRODUCTION

1.1 BACKGROUND

Wood-polymer composites (WPCs) have been commercially available since the 1960's, but they have mostly been reinforced with sawdust or wood powder which behave as fillers and thus lack any reinforcement capability [1]. Natural cellulosic fibers such as wood pulps behave as better reinforcing agents in composites due to their high strength and large aspect ratio [2]. Furthermore, recent developments in cellulose pulp processing have made nano-sized cellulose fibrils commercially available and this could promote their use as reinforcements in composite materials [3–5]. The high stiffness and strength, large surface area and high aspect ratio of the nano-scale cellulose fibrils have made them a viable option in composite applications [6,7]

Nevertheless, cellulose also has its drawbacks, especially in terms of being a natural material which leads to an inconsistent size of fibers/fibrils compared to organic or synthetic reinforcements. Furthermore, the fiber-matrix adhesion can be inefficient while using the hydrophilic cellulose as reinforcements in a relatively hydrophobic thermoplastic matrix [7]. The non-uniform reinforcement dispersion, aggregation, fiber breakage, moisture uptake and the rather low thermal stability of cellulose are also factors limiting its use as an efficient reinforcement in thermoplastic polymers. The low thermal stability may lead to discoloration and it may limit the processing temperature and hence the types of matrix that can be used with cellulose reinforcements, all pointing towards the dependence of cellulose-based composites on the processing method [8].

1.2 WOOD-BASED CELLULOSE REINFORCEMENTS

Cellulose is nature's own reinforcing structure found in the cell wall of all plants as well as in some tunicates, algae and bacteria. It is composed of glucose monomers linearly chained together by β 1-4 glycosidic bonds. The cellulose chain has a linear configuration due to the intra-chain hydrogen bonding between the OH-groups and oxygen in the adjoining chains [9]. The stability, insolubility in water and high axial strength of cellulose are understood to be due to the strong intra- and inter-molecular hydrogen bonding of the chains. The chains form fibrous, semi-crystalline units as observed in the fibrils which contain both highly ordered and disordered regions and are embedded in an amorphous matrix consisting of lignin, hemicellulose, pectin and waxes. These fibrils play a critical role in maintaining the structural integrity of the cell wall and in turn that of the entire

plant or tree, but it is unfortunately not possible to melt process them due to their high molecular weight and the fact that they decompose before melting [10].

Depending on the source, wood contains mainly cellulose, hemicellulose, and lignin apart from a small amount of extractives. The wood fibers have a hierarchical structure which gives the possibility to obtain a variety of different reinforcing capabilities resulting in different properties. In order to utilize the hierarchical structure, a pulping process is necessary to separate the cellulose fibers from each other, and this can be either mechanical, chemical or both. The mechanical pulping process involves wood chips which are mechanically ground, using refiner discs, to extract a high yield of pulp fibers and fragments, and, if the chips are preheated it is known as thermomechanical pulp (TMP). TMP contains cellulose, lignin, hemicelluloses and some extractives and its properties depend on the processing conditions used, which determine the fiber length and distribution [11]. In chemical pulp, the lignin which binds the fibers are dissolved using either the Kraft process or sulphite process. If the chemical pulp is extensively processed, and has a high cellulose content, a very low amount of other components and a low molecular weight, it is called dissolving pulp (DP) [12].

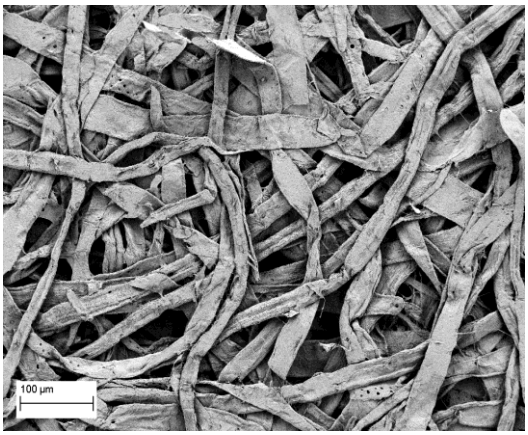

(a)

Figure 1: *Scanning electron micrograph of dried pulp fibers.*

If the fibers are further fibrillated or separated from each other so that at least one of the dimensions is on a nanometre scale, nanocellulose is obtained. The nanocellulose can be separated into cellulose nanofibers (CNF) and then processed further to cellulose nanocrystals (CNC). CNF contain both ordered (crystalline) and disordered (amorphous) regions with lengths up to a few µm [9]. Depending whether the fibrils are single or in bundles, their diameters vary from 3 – 5 nm to 15-20 nm [13]. Recent developments in pulp processing have reduced the energy demands to produce CNF, which are now available commercially [14]. They are produced by delamination of fibers either by intense mechanical treatment (homogenization with several passes) or by a combination

of chemical or enzymatical pre-treatment (introduction of charged groups) followed by homogenization [3]. The resulting suspension forms an aqueous gel at low concentration because of the increased surface area due to delamination and fibrillation, as shown in Figure 2.

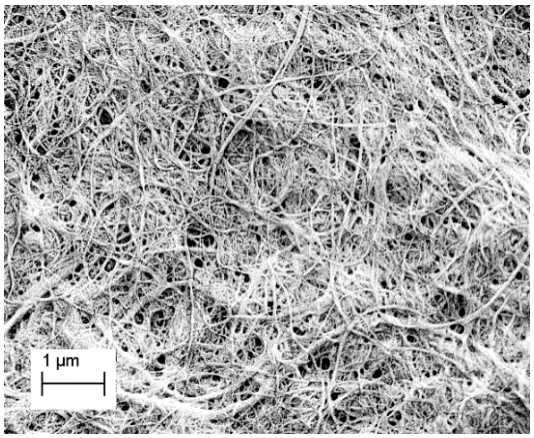

Figure 2: *Scanning electron micrograph of dried nanocellulose fibrils.*

Removal of the amorphous part of the CNFs by acid-catalysed hydrolysis gives cellulose nanocrystals (CNC) that are stiff, highly crystalline and rod-shaped, as shown in Figure 3 [15]. Their dimensions vary from 5-50 nm in diameter and 100-500 nm in length depending on their source and extraction method [16]. CNC in aqueous suspension can exhibit a liquid crystalline behaviour depending on the concentration, dimensions, ionic strength and type of counter-ion [13]. CNC suspensions also exhibit a gel-like behaviour but with a viscosity lower than that of the CNF due to the smaller aspect ratio of the nanoparticles. The main acids used to produce CNC's which are sulphuric acid and hydrochloric acid. The former creates CNCs functionalized with sulphate half ester groups which provide good colloidal stability but lower the thermal stability. On the other hand, hydrochloric acid produces CNC's with good thermal stability but poor colloidal stability due to the absence of charged species [17]. The CNCs have a tensile strength of 0.3-22 GPa and an axial modulus between 58 and 180 GPa, which makes them a promising candidate as a reinforcing element in composite materials [13,18]. Furthermore, CNCs have a large surface area accessible to modification by the addition of functional group which can reduce the hydrophilicity and the amount of accessible sulphate groups. The grafted chemical groups can improve the compatibility between the CNC's and the matrix material and increase the thermal stability as summarized by Börjesson and Westman [19].

Wood particles as reinforcement or filler in thermoplastics have been studied for decades [8,20,21], an understanding of the process and manufacturing of these materials is not well established, and their hydrophilic nature affects their ability to reinforce a hydrophobic polymer [8–10, 27]. As a reinforcement, efficient stress transfer plays a vital part in

improving the mechanical properties. Although nanocellulose has a high specific surface area, it also has a greater tendency to aggregate which undermines the realization of its true reinforcing capabilities.

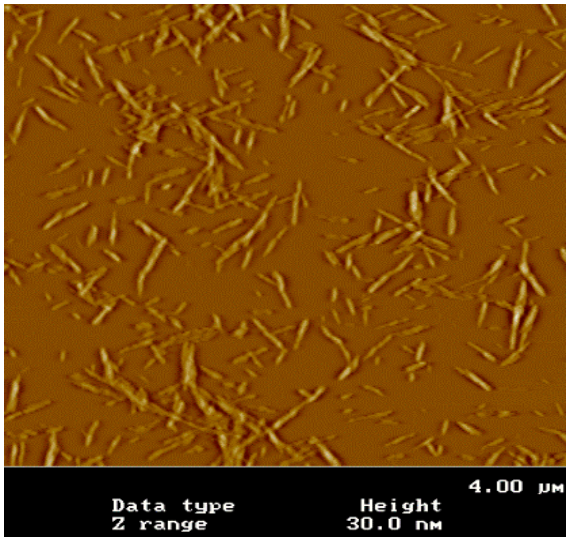

Figure 3: *Atomic force micrograph of dried nanocrystals.*

1.3 POLYMER MATRICES

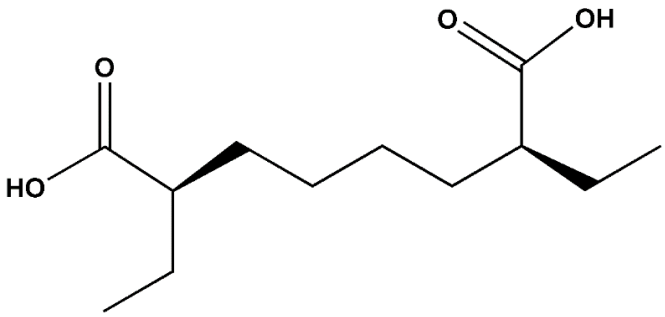

Figure 4: *Molecular structure of EAA with acrylic acid sections.*

In this study, a polyolefin in the form of ethylene-acrylic acid (EAA) or low-density polyethylene (LDPE) was chosen as polymer matrix. Poly(ethylene acrylic acid) (EAA) is an amphiphilic, semi-crystalline, random thermoplastic co-polymer which is used in coatings and packaging [24]. It consists of an ethylene backbone with random carboxyl pendants, as shown in Figure 4. The proportion of acrylic acid (AA) influences the physical properties of the polymer. The hydrophilicity increases with increasing AA content while the crystallinity is reduced, and the melting point drops. Thicker crystalline lamellae are obtained with lower AA content as there is less hydrogen bonding interfering with the

crystallization. EAA has been shown to be compatible with cellulose and its rather low melting temperature of 80 to 100 °C reduces the risk of thermal degradation of the additives [22]. Furthermore, the combination of properties such as flexibility, chemical resistance, and barrier properties of the ethylene with the polarity, toughness and hot tack strength of AA adds to the benefit of selecting EAA as a matrix [25]. As a reference that is commonly found in packaging materials, LDPE was selected.

1.4 PROCESSING OF CELLULOSE-REINFORCED COMPOSITES

The melt-processing of cellulose-based composites is not well understood, and much must be done to move towards large-scale application. The main method of producing nanocellulose composites has been through solvent casting, which so far has been only viable on a laboratory scale. In order to make the production of cellulose-based composites commercially interesting on an industrial scale, the feasibility of using a conventional melt processing technique should be considered [7,18,20,26–28]. A major drawback of using cellulose as reinforcement in thermoplastics is however the difference between the hydrophilic cellulose and the rather hydrophobic matrix phase. This incompatibility can affect the mixing of the cellulose in the matrix and can lead to aggregation of the cellulose fiber/fibrils resulting in a non-uniform thermoplastic composite [22]. Insufficient compatibility can also result in poor fiber–matrix adhesion, leading to poor stress transfer and inferior mechanical properties. The mechanical properties of cellulose composites are strongly dependent on the processing method used. Conventionally, cellulose polymer composites are produced either in a batch-wise process or in a continuous process. Batch-wise production is generally a laboratory-scale method such as solvent casting, micro-extrusion or resin impregnation, but these are difficult to scale-up to an industrial scale [7,26,29]. Large-scale industrial production is more likely to be feasible with a continuous process such as extrusion and injection moulding.

The continuous production of cellulose composites usually consists of two steps; the mixing of the reinforcing element with the matrix followed by a melt-shaping process such as compression moulding, extrusion or injection moulding. In the mixing step, a master-batch approach is usually used, where a dry mixture of nanocellulose is compounded with a polymeric carrier or compatibilizer, and this master batch is further diluted with the matrix polymer to obtain a raw material, such as pellets, that can be shaped [7]. The dewatering and drying of these cellulose nanomaterials tends however to promote irreversible bonding between nanofibers, and this can lead to undesirable aggregates in the composites [30]. It is a possible to break down the aggregates and improve their dispersion by repeated extrusion, but the high shear forces during the mixing/compounding operation can lead to thermal degradation [8,31–33]. To reduce the degree of aggregation, improve the dispersion and

reduce the degradation and discoloration of the composite, use of water-assisted extrusion might be employed in the compounding step [34]. Herrera et al. have shown that water-assisted extrusion improved the dispersion and mechanical properties of cellulose nanofibers and chitin nanocrystals in a polylactic acid matrix [34,35]. Another advantage may be that the discoloration can be reduced by the presence of water in the system [36–38]

The mixing can be done using either a single-screw or a twin-screw extruder (TSE), but the latter is preferred due to its superior mixing efficiency with both dispersive and distributive mixing and in some cases extensional mixing also. The twin-screw extruder is equipped with side feeding and vents which makes it possible to feed downstream of the melt and have better de-gassing capabilities, and this would make it feasible for liquid-assisted extrusion. The liquid-assisted technique can be considered as a useful way to disperse nanocellulose, as it is possible to use a large amount of water and, coupled with high shear forces, this should improve the dispersion of the reinforcement in the melt. This technique may also reduce the need for surface modification, the degradation of surface fillers and the 'blow up' phenomenon due to evaporation of pressurized water could further assist in dispersion. The water-assisted TSE method can make it possible to increase the cellulose loading to more than 50 wt% while maintaining good mechanical properties in the composite [22].

The pellets can be shaped into different profiles using compression moulding, single-screw extrusion or injection moulding. The shear forces generated in the shaping step decrease in the following order: injection moulding > single-screw extrusion > compression moulding. Single-screw extrusion always involves a certain amount of pressure and shear forces but in injection moulding, extensional flow fields and higher pressures act on the material apart in addition to the shear forces. This makes injection-moulded samples different from the single-screw extruded samples and compression-moulded samples [39]. Apart from the process parameters such as screw design, residence time, temperature and screw speed in the compounding step, the temperature, pressure, and time in the shaping step can also influence the final material properties.

1.5 AIM

The societal need for sustainable solutions has brought nanocellulose into the spotlight as a potential reinforcement in composite materials. However, the lack of concrete knowledge of the impact of the process parameters limits the industrial realization of these nanocellulose-based composites. The overall aim of the project was to improve the understanding of the melt-processing of cellulose nanocomposites while clarifying how the process structure and process parameters affect the properties of lignocellulosic-reinforced composites. The impact of the type of melt-processing technique on the properties of unmodified and modified nanocellulosic reinforcements has also been explored in order to assess the feasibility of up-scaling. Special emphasis was placed on wet-based melt-processing techniques in order to address the pre-existing issues of aggregation, dispersion and poor interfacial properties of the composites.

2 MATERIALS

The composites were prepared using cellulosic reinforcement at different hierarchical levels i.e., pulp fibers, cellulose nanofibers (CNF) and cellulose nanocrystals (CNC), with poly(ethylene-co-acrylic acid) (EAA) containing different amount of acrylic acid and low-density polyethylene (LDPE) as polymer matrix. The EAA was expected to be more compatible than LDPE with the cellulose-based reinforcements. The lower melting point of the EAA could also be beneficial, avoiding the degradation of the reinforcement. The LDPE is a commonly used polymer which is also available in bio-sourced grades [40].

2.1 CELLULOSE NANOFIBERS (CNF)

The CNF used in papers I and III was obtained from Borregaard A/S, Norway. The Exilva type material, obtained from Norwegian spruce sulphite pulp, for these CNFs was provided in the form of a 10 wt.% paste (Paper I) and a 2 wt% suspension in water (Paper III). The weight fractions of the cellulose, hemicellulose and lignin were found to be 94 wt%, 2.8 wt% and 3.2 wt%, respectively.

2.2 CELLULOSE NANOCRYSTALS (CNC)

In Papers II, III and V, sulphuric-acid-hydrolysed cellulose nanocrystals (CNC) were used as reinforcement. The CNC in Paper II was prepared in-house but the CNC in Papers III and V were obtained commercially. The CNC in Paper II was obtained using a procedure described by Hasani et al.[41] via acid hydrolysis of microcrystalline cellulose (MCC), Avicel® PH101, having an average particle size of 50 μm. In Paper V, spray-dried, water-dispersible powder of acid-hydrolysed cellulose nanocrystals was obtained from Celluforce, Canada. The powder was dispersed in water to obtain a CNC suspension having a solids content of 6-7 wt%, by mixing it using an IKA T25 digital Ultra Turrax at 7400 rpm for 10 min.

2.3 PULP FIBERS

The cellulose fiber pulp used as reference in Paper I was provided by Nordic Paper Seffle AB, Sweden. The pulp was a highly-beaten never-dried bleached softwood mixture of 80 % spruce sulphite and 20 % spruce sulphate pulps. The weight fractions of the cellulose, hemicellulose and lignin were 80 wt%, 17 wt% and 1.9 wt%, respectively, according to carbohydrate analysis. In Paper IV, thermomechanical pulp (TMP), from StoraEnso, Hyltebruk, Sweden and bleached-kraft dissolving pulp from Bahia Pulp S.A., Camacari,

Brazil were used. The source of the TMP was from Norwegian spruce and, according to the literature it had around 50 % of polysaccharides and around 30-35 % lignin [42,43] with a mean fiber length, fiber width and fines content of 3.2 mm, 35 μm and 33 % respectively, as measured by fiber analysis. The DP was obtained from eucalyptus, with an average degree of polymerization of 1340, and a mean fiber length, fiber width and fines content of 0.8 mm, 11 μm and 24 %, respectively, as measured by fiber analysis.

2.4 LUBRICANTS

The lubricants, molybdenum disulphide (MoS_2) and magnesium stearate (MgSt), used in Paper IV, were obtained from Sigma Aldrich. According to the supplier, MoS_2 was not exfoliated and had a density of 5,06 g/ml and the particle size was less than 2 μm, whereas the MgSt had a density of 1.026 g/cm^3 and a melting point of 200 °C.

2.5 ETHYLENE-ACRYLIC ACID COPOLYMER (EAA)

The ethylene-acrylic acid copolymer (EAA) dispersion used in Papers I, II, III and IV was obtained from BIM Kemi AB, Sweden. This grade had an acrylic acid content of 15 %, a melting point of 88 °C, a density of 0.994 g/cm^3 and a melt flow rate of 36 g/10 min (ISO 1133, 190 °C, 2.16 kg) according to the supplier. The aqueous dispersion had a solids content of 20 wt% and a pH of 9.7.

The EAA pellets used in Papers III and V was an ethylene-acrylic acid copolymer (EAA7), Primacor 3540, from Dow Chemical Company, with an acrylic acid content of 7 %. This EAA grade had a number average molecular weight (M_n) of 16100 g/mol, a density of 0.932 g/cm^3, a melting point of 95 °C and a melt flow rate (ISO 1133) of 8 g/10 min.

2.6 LOW DENSITY POLYETHYLENE (LDPE)

In paper V, a LDPE grade 19N730 from Ineos Olefins and Polymers, having a density of 0.92 g/cm^3, a melting point of 108 °C and a melt flow rate of 8 g/10 min (ISO 1133), according to the supplier, was used.

MATERIALS DESCRIPTION

Sample designations and preparation.

Cellulose nanocrystal reinforced composites	
Dispersion of ethylene-acrylic acid co-polymer (with 15 % acrylic acid content), mixed with 0.1, 1 and 10 **wt% cellulose nanocrystals, produced from microcrystalline cellulose**, surface modified with three different groups using hydroxyazetidinium salts: AzOH-Morpholine, AzOH-diHexyl and AzOH-diAllyl. Dispersion-mixed, air-dried and compression-moulded (Paper II)	EAA EAA-0.1 % CNC EAA-0.1 % MorphCNC EAA-0.1 % diAllylCNC EAA-0.1 % diHexylCNC EAA-1 % CNC EAA-1 % MorphCNC EAA-1 % diAllylCNC EAA-1 % diHexylCNC EAA-10 % CNC EAA-10 % MorphCNC EAA-10 % diAllylCNC EAA-10 % diHexylCNC
Dispersion of ethylene acrylic acid copolymer with 7 % or 15 % acrylic acid content, mixed with 10 **wt % cellulose nanocrystals from CelluForce**, surface modified with diAllyl using hydroxyazetidinium (AzOH-diAllyl) or a carbonate reagent. Processed as in Paper II (reference)	EAA-10 % CNC EAA-10 % diAllylCNC EAA7-10 % CNC EAA7-10 % diAllylCNC
	EAA-10 % diAllylCNC (Carbonate modified)
Pellets of ethylene acrylic acid copolymer with 7 % acrylic acid content, reinforced with 10 **wt%** Cellulose nanocrystals from CelluForce, surface modified with diAllyl using a carbonate reagent. Water-assisted extrusion and compounding in a twin-screw extruder followed by injection-moulded (Paper V)	EAA7 EAA7-10 % CNC EAA7-10 % diAllylCNC
	LDPE LDPE-10 % CNC LDPE-10 % diAllylCNC

Cellulose nanofiber and pulp-fiber reinforced composites	
Compression moulding of a dried mixture of a dispersion of ethylene acrylic acid copolymer (with 15 % acrylic acid) with cellulose nanofibers and pulp at various **vol%** (Paper I)	EAA
	EAA-CNF-10 to EAA-CNF-70
	EAA-Pulp-20
	EAA-Pulp-50
	EAA-Pulp-70
20 **vol%** nanocellulose pellets of ethylene acrylic acid (with 7 % acrylic acid) and master-batch of ethylene acrylic acid (with 15 % acrylic acid) and nanocellulose. Dispersion-mixed master-batch, compounded three times using different screw configuration (S1 & S2) in a twin-screw extruder and single-screw extruded into strips using different barrier screw profiles (M & B) (Paper III) *Designation - 'CNF- 2P- S1-M'* *A sample containing 20 vol% CNF, compounded twice in the twin-screw extruder using S1 screw design and shaped with the Maddock type barrier*	EAA7
	CNF-1P-S1-M
	CNF-2P-S1-M
	CNF-3P-S1-M
	CNF-1P-S2-M
	CNF-2P-S2-M
	CNF-3P-S2-M
	CNF-1P-S1-B
	CNF-2P-S1-B
	CNF-3P-S1-B
	CNC-1P-S2-B
	CNC-2P-S2-B
	CNC-3P-S2-B
Dispersion of ethylene acrylic acid copolymer (with 15 % acrylic acid content), mixed with 20, 50 and 70 **wt% thermomechanical pulp and dissolving pulp with and without lubricants. The lubricants were magnesium stearate and molybdenum disulphide at different concentrations.** Dispersion-mixed, air-dried and compression-moulded (Paper IV)	EAA
	DP or TMP30, 50, 70
	TMP30-MgSt, 5MgSt | DP30-MgSt
	TMP30-MoS_2, 5MoS_2 | DP30-MoS_2
	TMP30-MgSt+MoS_2 | DP30-MgSt+MoS_2
	DP or TMP50-MgSt
	DP or TMP50-MoS_2
	DP or TMP50- MgSt+MoS_2
	DP or TMP70-MoS_2
	DP or TMP70-MgSt

3 METHODS

The various experimental methods used to characterize the materials are listed here. Detailed descriptions are available in the appended Papers.

3.1 SURFACE MODIFICATION OF CNC

The surface-grafted modified CNCs were prepared by two different routes.

In Paper II, aqueous CNC dispersions were obtained using the method described by Sahlin et al. [44], which is a modification of previously outlined procedures [41,45]. In this case, hydroxy azetidinium salts were reacted with the sulphate groups on the CNC to graft one of the three different chemical groups onto the cellulose surface: N-morpholino-3-hydroxyazetidinium, N,N-dihexyl-3-hydroxyazetidinium and N,N-diallyl-3-hydroxyazetidinium, giving materials denoted MorphCNC, diHexylCNC and diAllylCNC, respectively.

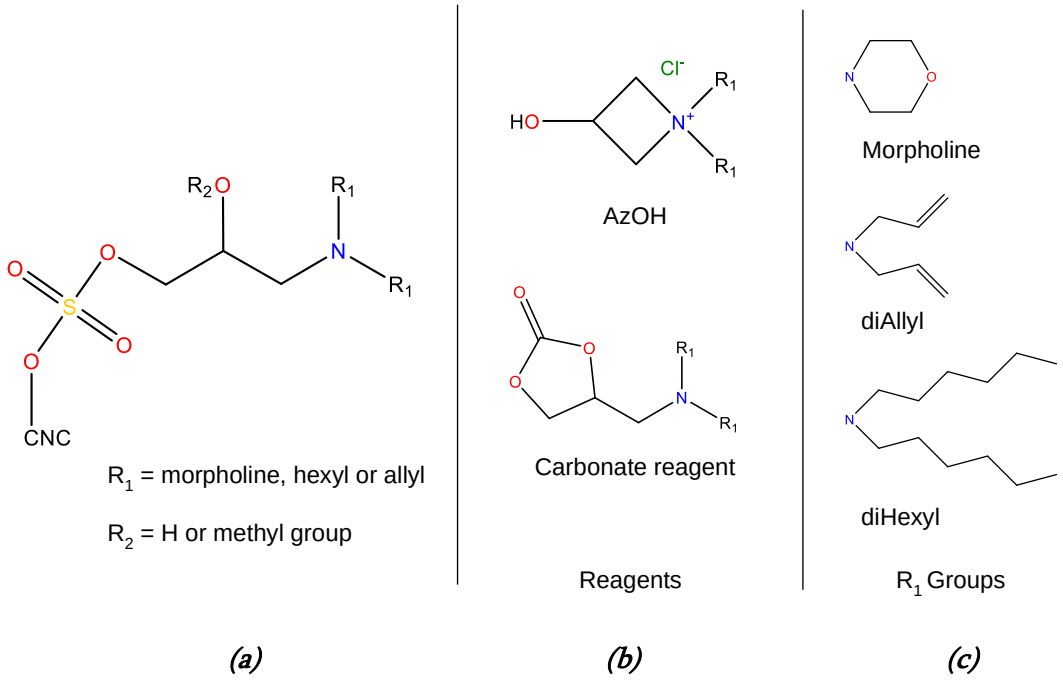

Figure 5*: Schematic view of the* ***(a)*** *surface-grafted CNC achieved using one of the two reagents in* ***(b)*** *and* ***(c)*** *the molecular structures of the different grafting groups, R1.*

In Paper V, the focus was on the upscaling of the CNC modification process with the most promising modified CNC (diAllylCNC). Due to the difficulty in producing large quantities of hydroxy azetidinium salts, the modification in Paper V was performed using the Celluforce CNC (see section 2.1) and the cyclic carbonate reagent (4-

z(diallylamino)methyl)-1,3-dioxolan-2-1), the synthesis being performed using a two-step reaction outlined by Reddy and Parzuchowski [46,47].

No significant changes were observed in the dimensions and weight of the modified CNC based on the type of grafting [41,48]. The synthesis of the azetidinium salts is described in detail in Paper II and V.

3.2 COMPOSITE MANUFACTURING PROCESSES

The melt processing techniques used in Papers I-V are listed in Table 1, their main differences being indicated in the respective sections.

Table 1: *Compounding and shaping techniques for the composite materials used in this work*

Paper	Mixing and compounding		Shaping		
	Dispersion mixing	Twin-screw extrusion	Compression moulding	Single screw extrusion	Injection moulding
I	X	-	X	-	-
II	X	-	X	-	-
III*	X	X	-	X	-
IV	X	-	X	-	-
V	-	X	-	-	X

*Master-batch approach

3.2.1 Dispersion mixing

Table 2: *Types of reinforcement and loading contents in the composite materials used in this thesis*

Paper	Reinforcement type and content		
	CNF	**CNC**	**Pulp**
I	10 – 70 vol%		20, 50, 70 vol%
II		0.1, 1, 10 wt%	
III	20 vol%	20 vol%	
IV			30, 50, 70 wt.%
V		10 wt.%	

In Papers I – IV, aqueous dispersions of EAA were mixed with the CNF (Papers I, III), pulp fibers (Papers I, IV) and CNC (Papers I, II, III) to achieve the loading contents shown in Table 2. All the CNF- and pulp-reinforced composites (Papers I, III and IV) were prepared via dispersion mixing using an L&W pulp disintegrator (Lorentzen & Wettre,

Sweden) at 2900 rpm for 20 min whereas the CNC-based composites (Papers II,III) were prepared using an IKA T25 digital Ultra Turrax at 7400 rpm for 6 min. In all cases, the suspensions containing the EAA dispersion, the cellulosic reinforcement and water (total water content 96 ± 1 %) were mixed and dried at room temperature before the composites were shaped.

3.2.2 Melt compounding by twin-screw extrusion

Master-batch approach

In Paper III, a master-batch containing nanocellulose (CNF or CNC) and EAA was prepared via dispersion mixing. The master-batch which contained 40 vol.% nanocellulose after being dried was compounded with EAA7 pellets to obtain a final nanocellulose content of 20 vol.% nanocellulose in the composite. The compounding was done using a co-rotating twin-screw extruder (TSE), Werner & Pfleiderer ZSK 30 M9/2 (Stuttgart, Germany), having a screw diameter of 30 mm and a screw length of 966 mm. The TSE had six heating zones including the die and an average throughput of 1.3 kg/h at 100 rpm. The temperature profile from the hopper to the die was 90–130–140–140–140–150 °C and the compounding was done three times using two different screw configurations (S1 & S2), as shown in Figure 6. The screw configurations had residence times of 7-8 minutes for the S1 screw, and 4-5 minutes for the S2 screw.

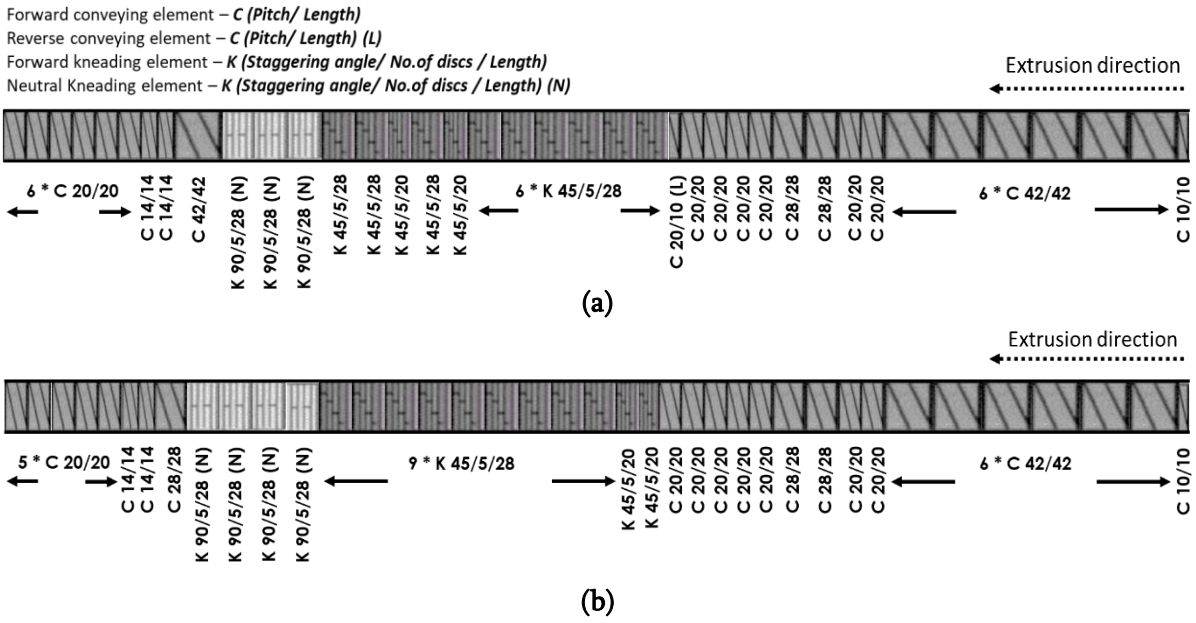

Figure 6: *The TSE screw configurations* ***(a)*** *S1 and* ***(b)*** *S2 used for master-batch compounding.*

Water-assisted extrusion

In Paper V, the same TSE was used in the production of CNC-based composites via water-assisted extrusion. In this case, a two-step approach was used where the material was

compounded twice using different screw configuration at each step. The first step was a water-assisted melt mixing using the mixing screw (MS) at 50 rpm, followed by a homogenizing extrusion (compounding) using a compounding screw configuration (CS) at 70 rpm. In the water-assisted melt mixing, the CNC suspension prepared from the Celluforce CNC (see section 2.2) was added into the hopper of the TSE together with the EAA7 or LDPE pellets. The unmodified CNC suspension was added into the hopper using a peristaltic pump (Heidolph SP standard, PD 5001, Schwabach, Germany) while a syringe was used for the more viscous diallyl-modified CNC. In all cases, the feed rates of the CNC and polymer pellets were adjusted to achieve a final CNC content of 10 wt% in the composite. The screw configurations used in the two-step water-assisted extrusion are shown in Figure 7. In Paper V, the TSE had a screw length of 971 mm and a temperature profile of 80-90-130-130-120-120 °C for the first pass (mixing step) and 120-140-200-200-170-170 °C for the second pass (compounding step). The residence time and throughput, were respectively, 7-8 min and 1 kg/h, for the MS screw configuration and 2-3 min and 3 kg/h, for the CS screw configuration.

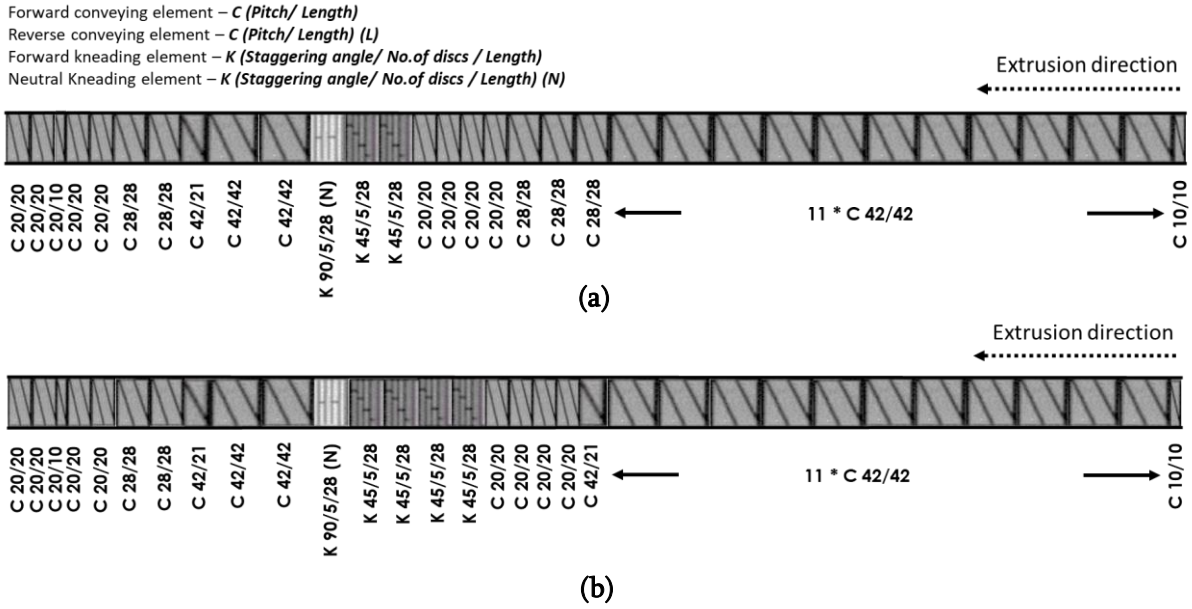

Figure 7: The TSE screw configurations used for water-assisted extrusion mixing and compounding **(a)** mixing screw (MS) and **(b)** compounding screw (CS)

3.2.3 Shaping

Compression moulding

In Papers I, II and IV, the dried EAA/cellulose samples were finally shaped using a Buscher-Guyer KHL 100, Switzerland. A minimum of 12 g of dried sample was used to produce square plates 100 x 100 mm^2 in size and about 1 mm thick. The compression moulding was carried out at 105 °C with a maximum pressure of 50 MPa and a compression moulding

cycle time of approximately 10 minutes. A more detailed description of the moulding procedure is given in Papers I, II and IV.

Single-screw extrusion (SSE)

In Paper III, the pellets were shaped using a Brabender single-screw extruder, Brabender OHG, Duisburg, Germany, with a screw diameter (D) of 19 mm and a screw length of 25D. The temperature profile from the hopper to the die was 90-130-140-150 °C, and the screw rotation rate was 30 rpm. A die with a width of 100 mm and a slit height of 1 mm was used to produce flat films. The shaping was performed using barrier screws with two different screw profiles, a Maddock type barrier screw (M), having a compression ratio of 2:1, and a Maillefer type barrier screw (B), having a compression ratio of 2.5:1 with a Saxton type distributing mixing profile.

Injection Moulding (IM)

In Paper V, the final shaping of the upscaled CNC-containing composites was carried out using an injection moulding machine, Arburg Allrounder 221M-250-55 (Austria), producing test plates with dimensions of 64 x 64 x 1.5 mm^3. The temperature profile from the hopper to the nozzle was divided into five heating zones along the barrel; 110-150-150-170-170 °C, the injection pressure was 5 MPa and the mould temperature was 25 °C. The circumferential screw speed was set to 20 m/min with a holding pressure and back pressure of 80 MPa and 1.5 MPa, respectively. The sprue from the cylinder nozzle to the cavity had a diameter which varied along a length of 54 mm from 4 mm to 7 mm. This was followed by an 18 mm long runner with a cross section of 40 mm^2 and a rectangular cavity gate having an 8 x 1.5 mm^2 cross section and a land length of 1 mm. The injection speed was 50 cm^3/s when filling the sprue, and 20 cm^3/s when filling the mould cavity. The injection moulding cycle time was 45 s, including 10 s holding time and 30 s cooling time. For each sample series, the first 20 injection-moulded samples were discarded, before the process was considered to have reached a steady state.

3.3 CHARACTERIZATION METHODS

3.3.1 Characterization of reinforcements and CNC surface grafting

Detailed descriptions of the methods employed for the CNC characterization are given in Papers I -V. Brief descriptions are given here.

In Papers I and IV, the length and width of the reinforcements were determined using a Kajaani FS300 fiber analyser (Metso Automation, Finland) according to the Tappi T271

standard. The fiber length and fiber width were taken as the averages of 25000-30000 fiber pieces. In Papers I and III, the dimensions of the CNF and CNC were evaluated from a 10-ppm dried dispersion using atomic force microscopy (AFM) in the tapping mode (Nanoscope IIIa with a Micro Masch silicon cantilever NSC 15 with a type G scanner, Digital Instruments Inc.).

The ζ-potential of the surface-grafted CNC was determined using a Zetasizer Nano ZS (Malvern Instruments, UK) based on the Laser Dopple Velocimetry technique. The measurements were performed at 25 °C on a 0.05 wt.% CNC suspension using DTS1070 disposable folded capillary cells, with a 50 mW diode-pumped solid-state laser with a wavelength of 532 nm as light source.

The sulphate half ester content was determined following the procedure described by Foster et al [49] using conductometric titration. 100 ml of a CNC dispersion having a concentration of 0.1 wt% was prepared and titrated with a 10 mM sodium hydroxide solution (standardised against potassium hydrogen phthalate) added in 100 μL aliquots at 30 second intervals until the required number of data points had been collected.

Attenuated total reflectance Fourier-transform infrared spectroscopy (ATR-FTIR) was performed using a Perkin Elmer Frontier FT-IR Spectrometer (Waltham, MA, USA) equipped with a diamond GladiATR attenuated total reflectance (ATR) attachment from Pike Technologies. The dried CNC films and the pulp composites (Paper IV) samples were placed directly on the ATR-crystal without further preparation. The spectra were recorded between 4000 and 400 cm^{-1} and 20-32 scans were collected.

3.3.2 Appearance and microstructure of the composites

The Malvern Instruments Zetasizer ZEN3600 was used to measure the hydrodynamic diameter of the milky white EAA dispersion at room temperature after diluting it to 0.01 wt.% with deionized water and sonication. The morphology of the dried CNF suspension (Paper I) and the cross section of cryo-fractured composites (Paper III) were assessed by scanning electron microscopy (SEM) using LEO ULTRA 55 FEGSEM on gold sputtered samples. In Paper IV, FEI Quanta 200 FEG ESEM was used to assess the morphology of the fibers and of the cross section of cryo-fractured composites followed by an elemental composition analysis through energy dispersive X-ray analysis (EDX) on the lubricated fibers. In Paper III, the presence of aggregates in the extruded films was investigated using a stereomicroscope (SteREO Discovery V20 from Carl Zeiss, Germany). Images from three different regions of the extruded film were studied.

In Paper V, the color of the composite materials was determined using a Datacolor 600 spectrophotometer with a 9 mm diameter opening and a d/8° spherical measurement geometry. The color was expressed in the 1976 CIELAB system ("ISO/CIE 11664-4:2019," 2019) with coordinates L^*(lightness), a^*(red-green) and b^*(yellow-blue). The gloss of the composite materials was measured with a Konica Minolta Uni Gloss 60Plus or a BYK Gardner-micro-TRI-gloss with an angle of incidence of 60 ° at room temperature.

In paper I, the dispersion of the composite was evaluated from a 3D interpretation of the internal structure of the composites using a Zeiss Xradia XRM520 X-ray tomograph. The scanned composite volume was reconstructed into voxels with a size of 1 μm^3. Since a 16-bit gray scale can be used to show the density of the material, a voxel gray scale was generated using the ImageJ software. Based on surface reconstructions, a 3D image of the composite internal structure was made in 3D slicer.

3.3.3 Thermal Properties

Thermo-gravimetric analysis (TGA) was employed to assess the thermal stability of the materials using a TGA/DSC 3 + Star system (Mettler Toledo, Switzerland). The samples were subjected to a heating ramp from 25 °C to 500 °C at a rate of 5 °C/min or 10 °C/min in a nitrogen atmosphere.

In Paper II, the thermal stability of all the composites containing surface-modified CNC was assessed visually using the Kofler bench. Reference samples, surface-treated and untreated composite samples with 10 wt.% CNC were held at 120, 130, 140, 150 and 160 °C for 8 minutes in order to determine the temperature at which discoloration occurred. Similarly, a comparison was also made between the pH-neutralized 10 wt% CNC-diAllyl-OH and the 10 wt% untreated CNC composites.

In order to identify the thermal transitions and assess the crystallinity of the composite materials, differential scanning calorimetry (DSC) was employed using a Perkin-Elmer DSC7 or a Mettler-Toledo DSC 2. The endotherms were recorded while the temperature was increased from -20 to 250 °C at a rate of 10 °C/min in a nitrogen atmosphere.

3.3.4 Rheological properties

The rheological properties of both the EAA-CNF suspensions (with two different CNF concentrations) and the CNF suspension were assessed in Paper I using an Anton Paar MCR 702 Rheometer (Graz, Austria). The suspensions were measured with an oscillating shear strain of 0.1 – 100 % strain at 1 Hz and at a steady shear flow (0.1 – 100 s^{-1}) at 25 °C, followed by temperature sweep measurements between 27 and 90 °C at 1 Hz and a strain amplitude of 0.2 %. The shear strain and the viscosity were measured with a cone-plate configuration

having a plate diameter of 25 mm and a gap of 0.106 mm, and a parallel plate fixture with a diameter of 15 mm and a gap of 0.5 mmm was used for the temperature sweep tests. In each case, the storage modulus *G'* and the loss modulus *G"* were determined.

Small-amplitude oscillatory shear tests (SAOS) were performed on the shaped composites in Papers III, IV and V. The disk-shaped samples were analysed using a parallel plate geometry (15 mm plate diameter) at 150 °C (Paper III) and 170 °C (Papers IV and V) during which the composites were found to be stable for a period of more than 50 minutes. Thermal degradation during the rheological measurements was considered to be negligible. In the SAOS experiments, the linear viscoelastic region was therefore first assessed using a strain sweep from 1 to 100 % at a constant angular frequency of 1 s^{-1}. In addition, angular frequency sweeps in the range of 0.08–200 s^{-1} were performed at strain amplitudes of 0.04 - 0.7 %.

In Papers III and IV, steady shear viscosity measurements were also performed on the composite melts using a parallel-plate fixture in the shear rate range from 0.1 to 10 s^{-1}. In Paper V, a capillary viscometer (Göttfert Rheograph 2002, Germany) was used to measure the shear viscosity of the 10 wt% CNC samples as a function of shear rate at a melt temperature of 170 °C. Two cylindrical capillaries with similar diameters (1 mm) but different lengths (10 and 20 mm) were used to estimate the pressure losses at the entrance (Bagley correction of the applied pressure). The applied pressure when pushing the melt through the capillary at different piston speeds was recorded using a 50 MPa pressure transducer (Dynisco, USA). The piston speed was varied between 0.05 and 2 mm/s, corresponding to shear rates of 58 to 2300 s^{-1}. The measured shear rates were subjected to the Rabinowitsch-correction.

3.3.5 Tensile properties

The mechanical properties of the shaped composites were measured in tension using a Zwick/Z2.5 tensile tester with a 500 N (Paper II) and 2 kN (Papers IV, V) and a Zwick Z1/ Roell with a 1 kN load cell and a Zwick Eye UI 1540M video extensometer (Papers I, III). Test bars with a gauge length and width of 20 and 4 mm, respectively, were used as required by the ISO 527-3 standard. The samples had an approximate thickness of 1 mm and were kept in a conditioning chamber at 23 ± 2 °C and 50 ± 5 % relative humidity for at least 48 hrs, prior to the tensile tests. The tensile properties were measured at 23 ± 2 °C at a strain rate of $2.5 \cdot 10^{-3}$ s^{-1} (6 mm/min). In Paper I, the effective stiffness of the CNF-reinforced composites was determined according to the Halpin-Tsai model, and the Cox-Krenchel model was used to compare the tensile moduli (Papers I, II). A detailed explanation is given in the appended papers.

3.3.6 Dynamic-mechanical analysis

A Rheometrics RSA II was used to measure the dynamic-mechanical properties of the materials. In Paper I, the thermo-mechanical properties of the composites were measured by an initial strain sweep followed by a temperature sweep in the range of -80 to 110 °C at a strain amplitude between 0.1 and 0.15 %. In Papers II – V, the interphase properties of the composites were studied by applying a constant tensional strain of about 0.13-0.15 % while a sinusoidal deformation was superimposed at a constant temperature of 23 °C. The measured values of the storage modulus, the loss modulus and the mechanical loss factor were used to discuss the adhesion and relative stability of the interphase region between the matrix and the reinforcement.

4 SUMMARY OF RESULTS

The results are summarized with regard to the characterization of the reinforcement and the effects of the manufacturing process on the appearance and microstructure, and the thermal, rheological and mechanical properties of the composites.

4.1 CHARACTERIZATION OF REINFORCEMENTS

4.1.1 Dimensions

The dimensions of the reinforcements were analysed using fiber analysis (Papers I, IV) and AFM (Papers I, II, III), and they are given in Table 3. The CNF had fibers or large fiber fragments which were still present in the CNF starting material, as reported by Larsson et al.[50] on similar cellulose grades. As expected, the highly beaten never-dried pulp fiber (reference pulp in Paper I) had a higher fines content and smaller dimensions than the TMP based fiber.

Table 3: The dimensions of the cellulose reinforcements and the fines content measured by fiber analysis and AFM.

Cellulose Type	Length (*mm*)	Width (μm)	Fines (%)
CNF	0.34	18.4	78
Reference Pulp	1.36	24.4	11.9
TMP	3.2	35	33
DP	0.8	11	24
CNC (Paper II)*	6 ± 1.5 *nm*	211 ± 114 *nm*	-
CNC (Paper III)	6 ± 3 *nm*	301 ± 110 *nm*	-

***** Measured in other work using AFM [51]

4.1.2 Surface grafting of CNC

The CNC in Papers II and V was subjected to surface modification using either hydroxyazetidinium salts (Paper II) or a carbonate reagent (Paper V). In Paper II, the in-house CNC was modified using three different surface modification groups, Morph, diHexyl and diAllyl, whereas in Paper V, the diAllyl modification was used. During the upscaling of the process (Paper V), a cyclic carbonate reagent was used instead of the hydroxyazetidinium salts, the reason being that it was difficult to consistently produce on

a large scale, high purity salts required for the grafting. A similar grafting could be achieved using the carbonate reagent.

The surface grafting was characterized by FTIR, ζ–potential measurements, conductometric titration and thermal stability measurements (TGA) and a detailed explanation can be found in Papers II and V. The surface modification was confirmed by the shifts of the peaks in the absorption bands of the sulphate esters in the FTIR spectra, indicating sulphate ester substitution. The ζ-potential measurements gave lower values for the modified CNC (Paper II) suggesting a reduction in the amount of free sulphate groups due to grafting. Similarly, the conductometric titration (Paper V) showed a reduction in the surface charge for the modified CNC, suggesting a reduction in the negatively charged sulphate groups due to successful grafting on the sulphate half esters of the CNC.

4.2 APPEARANCE AND MICROSTRUCTURE OF THE COMPOSITE

The visual appearance and the morphology of the shaped cellulose reinforced composites were assessed in Papers I - V.

4.2.1 Visual Appearance

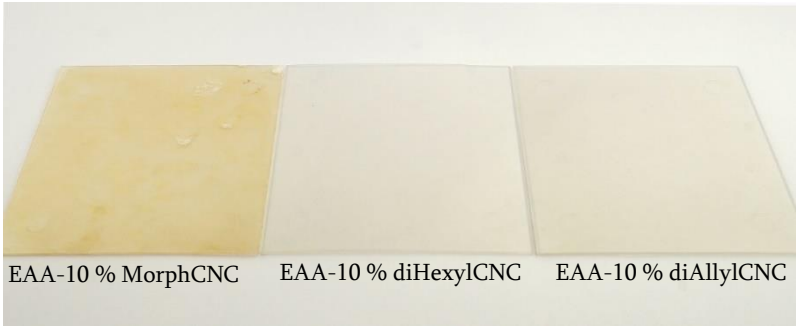

Figure 8: *Dispersion mixed, air-dried and compression-moulded EAA composites with 10 wt.% surface modified CNC.*

In Paper II, aqueous dispersions of CNC with the Morph, diHexyl and diAllyl modification groups were mixed with EAA with 15% acrylic acid (EAA) to produce composites containing 0.1, 1 and 10 wt.% CNC, as seen in Figure 8. The mixtures were then dried at room temperature, to minimize the tendency of the CNC particles to aggregate, and compression-moulded to obtain a well dispersed CNC composite material, as described by Venkatesh et al. [52]. With 10 wt% modified CNC, the composites with MorphCNC were more yellow in appearance than the transparent diHexylCNC and diAllylCNC reinforced samples. The discoloration of the EAA-10 % MorphCNC was not further investigated, but it has been suggested that the influence of amine structure could cause the yellowing

[53,54]. The CNC-modified composites showed no visible aggregates up to loading contents of 10 wt%.

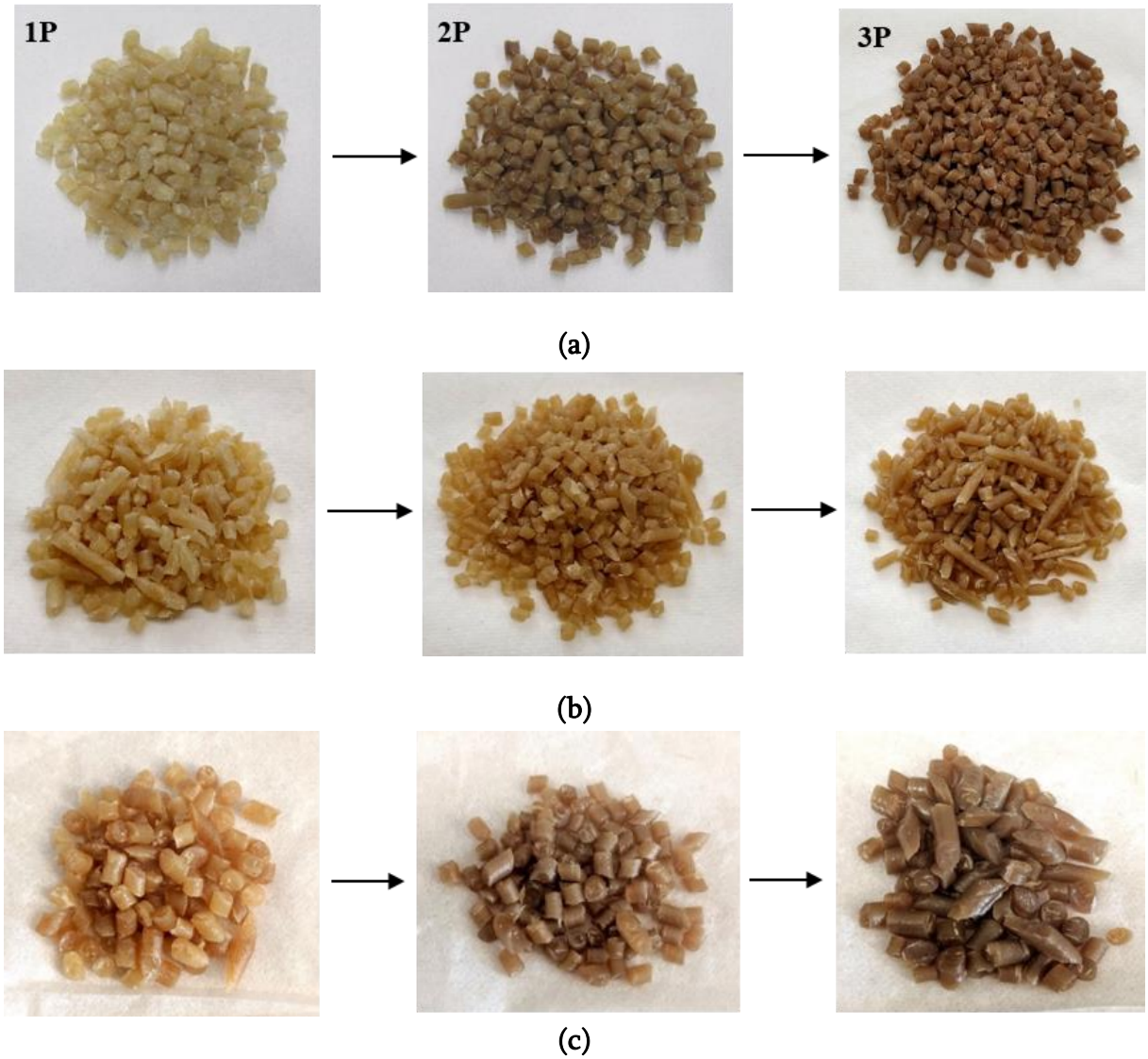

Figure 9: *Photographs of 20 vol.% **(a, b)** CNF- and **(c)** CNC-reinforced pellets compounded using **(a)** S1 and **(b, c)** S2 screw configuration, in TSE. The images show from left to right, a single-pass samples (1P), two-pass samples (2P) and three-pass samples (3P).*

In Paper III, the 20 vol% nanocellulose reinforced EAA7 pellets were obtained by compounding the master-batch (EAA+nanocellulose) with EAA7 using the TSE. The pellets showed a pronounced increase in discoloration with increasing number of passes through the TSE, as shown in Figure 9. The screw configuration played an important role in the discoloration, as the S1 screw configuration (longer residence time) led to a more pronounced discoloration than the S2 screw configuration (shorter residence time).

Although the residence time was short, the discoloration was probably due to the limited thermal stability of the CNC (to be discussed later in section 4.3.1).

Based on the findings in Paper II, an upscaling study to produce 3 kg batches of 10 wt% (diAllyl modified and unmodified) CNC-reinforced EAA or LDPE composites was considered (Paper V). In this case, the samples were produced using water-assisted extrusion using a TSE and injection moulding into plaques. A clear difference in transparency and color was apparent in the injection-moulded samples, as seen in Figure 10, along with the visible aggregates. The discoloration was greater in the EAA7 samples, especially those containing diAllyl-modified CNC. The reason for the discoloration is discussed further in section 4.3.1.

Figure 10: Injection-moulded composites with 10 wt.% CNC, compounded by water-assisted extrusion in TSE

Table 4 presents the color and gloss data for the injection-moulded plaques. A reduction in lightness (L*) was noted for CNC-reinforced samples compared to the unfilled matrix, particularly in the EAA7 composites. As seen in figure 10, the reinforced samples were more yellow (b^*) than the neat matrices and the addition of CNC to EAA7 resulted in a slight increase in the redness (a^*). A slight decrease in the gloss values relative to that of the unfilled material was probably due to the rougher surface after addition of the reinforcing element.

Table 4: *The color coordinates and gloss value of the injection-moulded composite materials and of the unfilled polymer matrices.*

	CIEL^*	CIEa^*	CIEb^*	Gloss (%)
EAA7	84.0	2.5	-3.5	26.9
EAA7-10 % CNC	58.9	4.7	21.3	19.9
EAA7-10 % diAllylCNC	52.2	6.0	19.2	21.7
LDPE	77.3	2.6	-4.6	26.7
LDPE-10 % CNC	68.2	2.2	13.2	22.8
LDPE-10 % diAllylCNC	69.1	0,9	13.2	26.1

4.2.2 Tomography

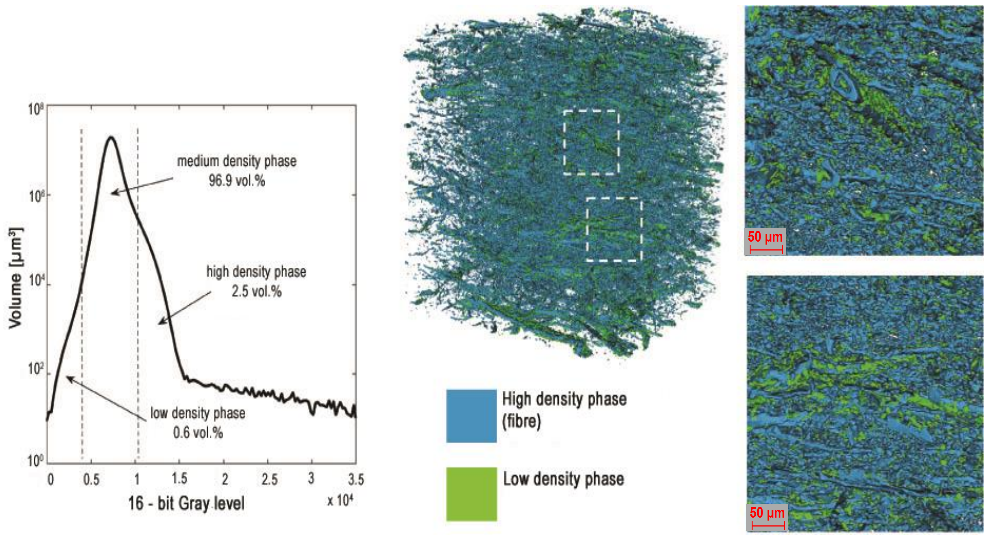

(a) (b)

Figure 11: *EAA–CNF-20* ***(a)*** *X-ray microtomography data showing three density phases for the EAA–CNF-20 material,* ***(b)*** *3D reconstruction of the (blue) high density fiber phase and of the (green) low density phase.*

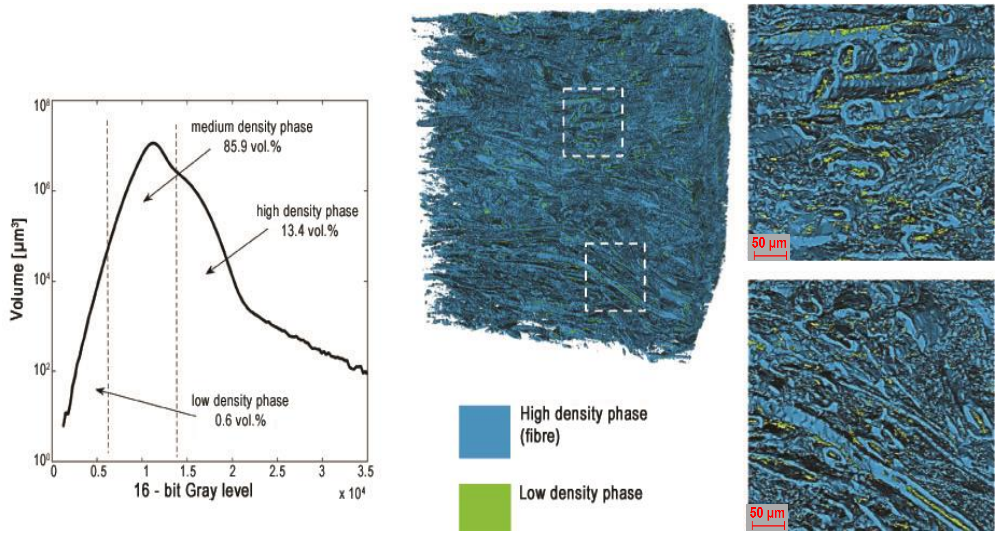

(a) (b)

Figure 12: *EAA–Pulp-20* ***(a)*** *X-ray microtomography data showing three density phases for the EAA–Pulp-20 material,* ***(b)*** *3D reconstruction of the (blue) high density fiber phase and of the (green) low density phase.*

In Paper I, X-ray microtomography was performed on the 20 vol.% CNF-EAA and pulp-EAA composites (containing 15 % acrylic acid) prepared by dispersion mixing and compression moulding. The microstructure was analysed from the 3D reconstructed samples, see Figures 11 and 12 by distinguishing three distinct phases based on the voxel gray scale which corresponds to density. As expected, a small fraction (2.5 vol.%) of cellulose fibers were observed for the 20 vol% CNF samples, seen as a phase with the highest voxel density, but the rest of the sample was hard to differentiate as the differences fell below resolution limit of the instrument (1 μm/voxel). The same was true for the highly beaten pulp fibers (see figure 12) which showed a higher content (13 vol%) of cellulose fibers than expected. The low-density phase distinguishable around the cellulose surface and in the lumen, probably represented amorphous EAA or voids.

4.2.3 Microscopy

In Paper III, the morphology of the specimen was affected by the screw configuration during compounding and the screw profile during shaping. The S1 screw configuration (longer residence time) and the Maddock barrier screw were more effective in reducing the size of the aggregates with increasing number of passes, see Figure 13 (a), (b) and (c), probably due to the high shear regions in the screws. The CNC samples, figure 13(d), exhibited an aggregate size smaller than that of the CNF-based samples, owing to the lower aspect ratio of the rod-like reinforcement.

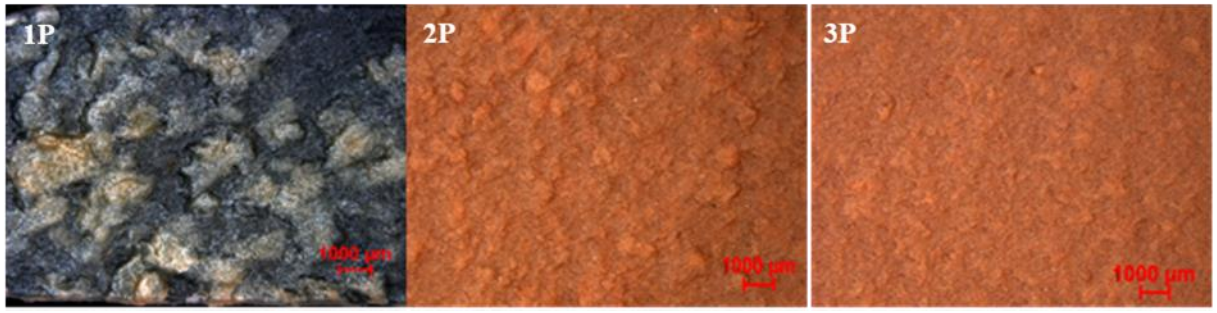

(a)

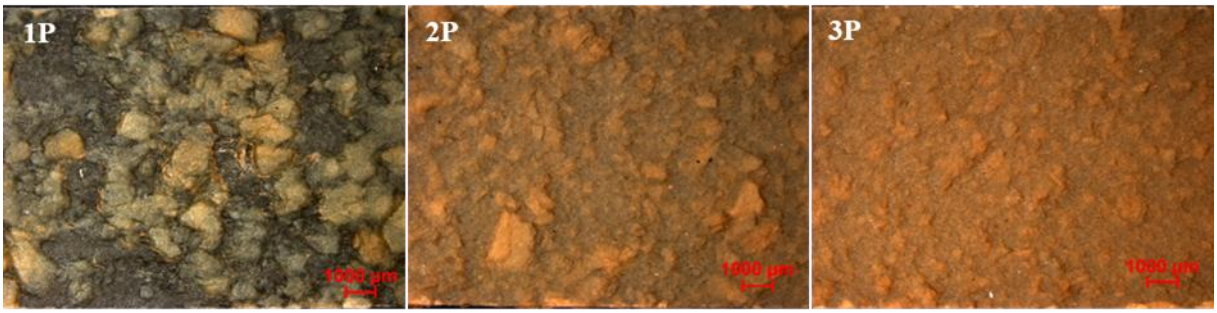

(b)

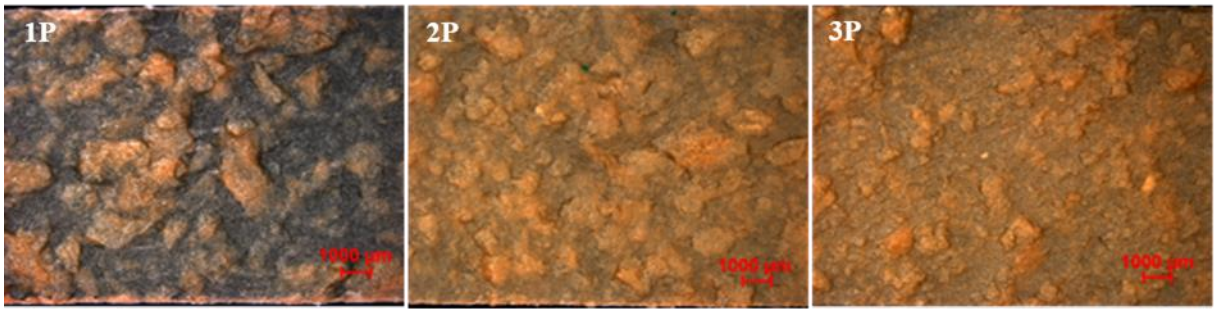

(c)

(d)

Figure 13: *Stereo-micrographs of 20 vol.% **(a, b, c)** CNF and **(d)** CNC-reinforced films compounded using **(a, b)** S1 and **(c, d)** S2 screw configurations, and shaped using the **(a, c)** Maddock type and **(b, d)** Maillefer type barrier screw.*

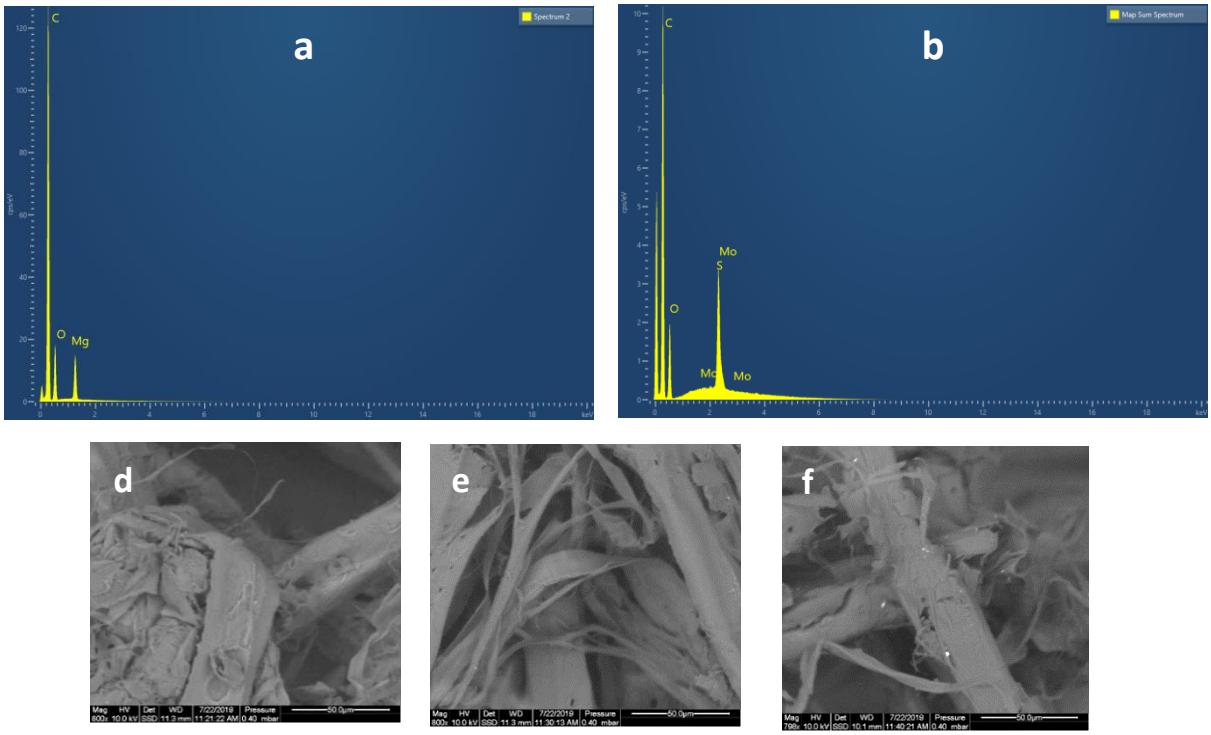

Figure 14: *EDX analysis of **(a)** 95 wt% TMP + 5 wt% MgSt and **(b)** 95 wt% TMP + 5 wt% MoS_2, and scanning electron micrographs of **(d)** TMP fibers **(e)** 95 % TMP + 5 % MgSt **(f)** 95 % TMP+ 5 % MoS_2, at a magnification of 800x.*

In Paper IV, SEM and EDX analysis were used to study the pulp fibers (TMP or DP) with 5 % lubricant (MgSt (magnesium stearate) or MoS_2 (molybdenum disulphide)) to assess the adsorption of additives. Figures 14(d-f), shows that the TMP with additives showed a smoother fiber surface in the presence of the lubricants but for the DP-containing samples the fibers appeared to be the same in all cases. This distinction was also clear in the EDX analysis of the samples, see Figure 14(a), where the peak positions indicated that the MgSt was adsorbed onto the TMP fibers, but that this was less clear for the DP with MgSt, see Figure 15(a). In the case of MoS_2, the TMP which contains aromatic lignin structures showed a greater adsorption than the DP [55].

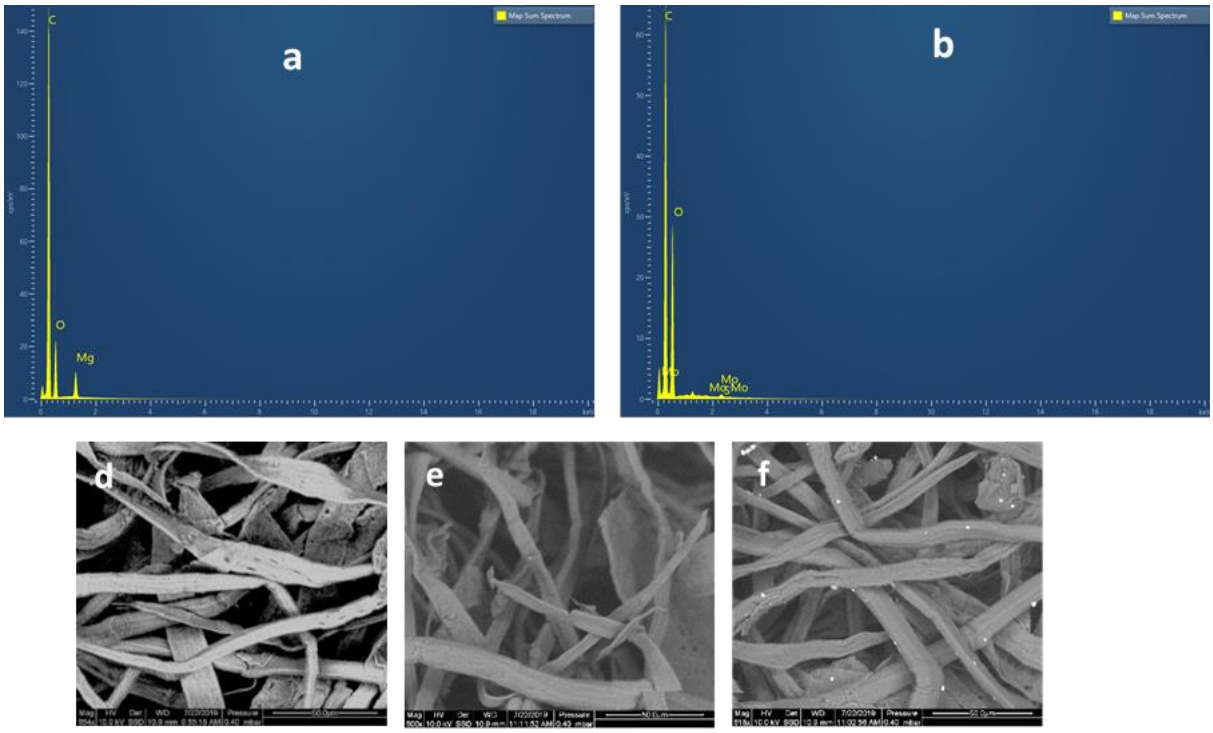

Figure 15: *EDX analysis of* ***(a)*** *95 wt% DP + 5 wt% MgSt and* ***(b)*** *95 wt% DP + 5 wt% MoS_2, and scanning electron micrographs of* ***(d)*** *DP fibers* ***(e)*** *95 % DP + 5 % MgSt* ***(f)*** *95 % DP + 5 % MoS_2 , at a magnification of 800x.*

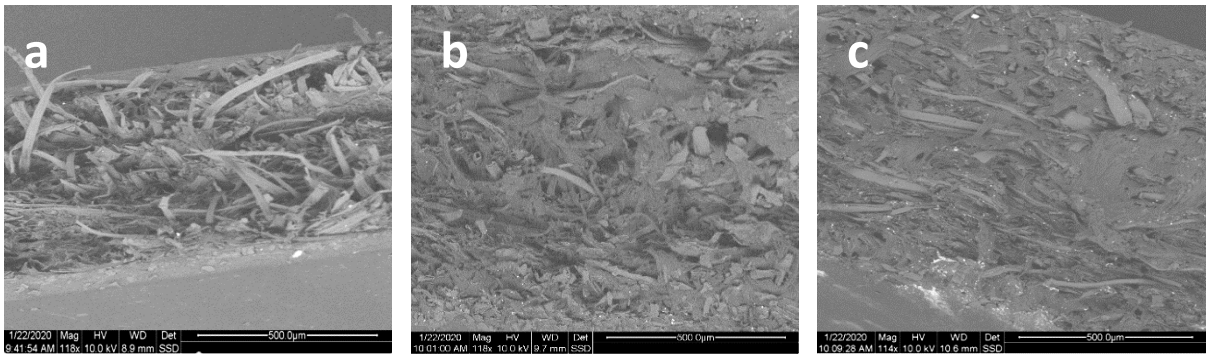

Figure 16: *Scanning electron micrographs of EAA samples reinforced with* ***(a)*** *30 wt% TMP (TMP30)* ***(b)*** *TMP30 with MgSt* ***(c)*** *TMP 30 with MoS_2, at a magnification of 115x.*

Cryo-fractured composite samples of EAA reinforced with 30wt% TMP (TMP30) were also studied, and it was seen that the addition of lubricants resulted in a more compact structure than that of the sample without lubricants, see Figure 16.

4.3 CHARACTERIZATION

4.3.1 Thermal properties

Thermogravimetric analysis was used to assess the thermal stability of the materials and it was the thermal stability of the CNC-based composites showed that showed the most interesting results. The onset of thermal degradation of the CNC samples is summarized in Table 5, and detailed information is available in the appended papers. In Paper II, that the onset of degradation of the grafted CNC was at a temperature almost 100 °C higher than its unmodified counterpart, as shown in Table 5 and Figure 17, probably due to the removal of the acidic hydrogen of the sulphate half ester which prevents catalytic degradation [44,56].

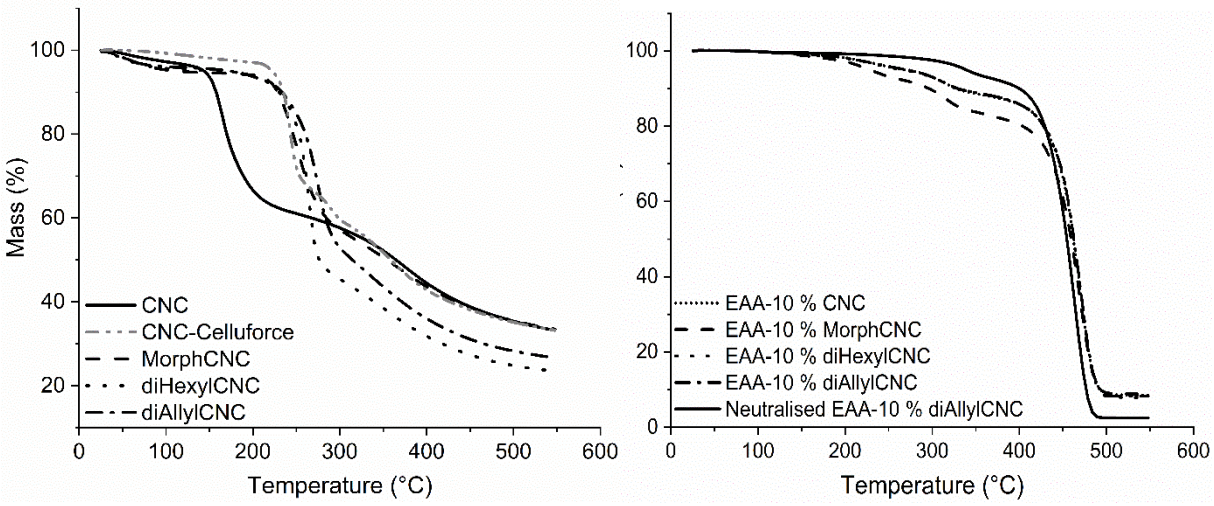

Figure 17: *Thermogravimetric curves showing the thermal degradation of* ***(a)*** *unmodified CNC and azetidinium-grafted CNC before mixing with polymer and* ***(b)*** ***of*** *their compression-moulded composites.*

However, when the EAA with 15 % acrylic acid composites reinforced with modified CNC (Paper II) were made via dispersion mixing and compression moulding, no improvement in thermal stability was observed. Figure 18 shows that the 10 wt% CNC composites placed on the Kofler bench at 120, 130, 10, 150 and 160 °C (for 8 minutes) changed color at about 150 °C. At 160 °C, all the composite samples were brown without no significant difference between the modified and unmodified CNC-based composites, and this was also confirmed by the TGA results (Figure 17b). However, with a pH-neutral 10 wt% composite containing

CNC-diAllyl-OH was studied, no significant color change was observed even at 160 °C, as seen in figure 18(b), and this was also confirmed by the TGA (Figure 17b). This discrepancy could be explained by the poor chemical stability of the sulphate diester, which acts as a good leaving group in the presence of hydroxides and carboxylate, in an alkaline environment (the pH of the EAA dispersion was 9.7). The azetidinium groups can thus be cleaved by the carboxylates of the EAA matrix and this in turn leads to the formation of sulphate half ester which is less stable. At neutral pH, however, the carboxylate is in the form of carboxylic acid which is less prone to react with sulphate ester and degradation occurs at a higher temperature. A similar discoloration was observed in the 20 vol% CNC-EAA7 composites in Paper III.

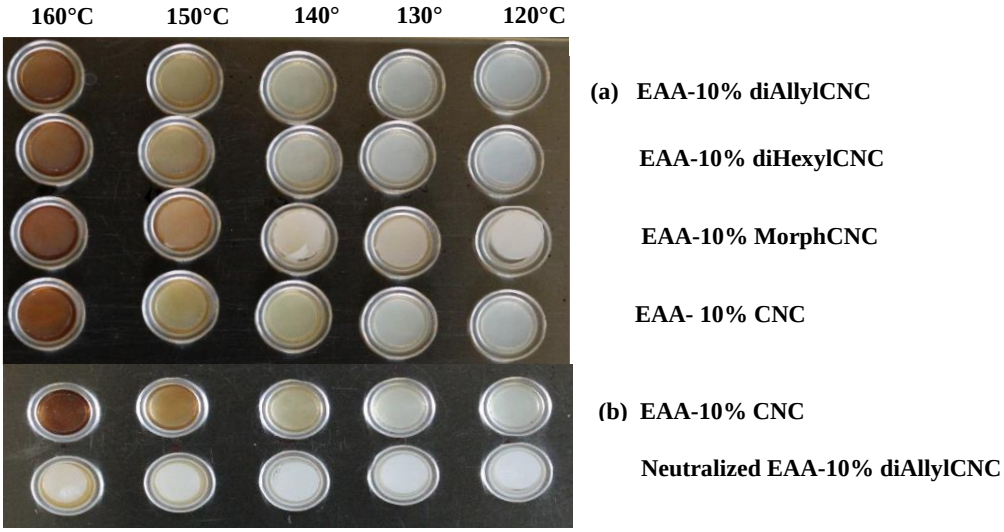

Figure 18: *(a) Visual appearance of the composites containing 10 wt% CNC after exposure for 8 minutes at different temperatures. (b) Visual appearance of the composites containing 10 wt% untreated CNC and 10 wt% CNC-diAllyl-OH from the pH neutralized system after exposure for 8 minutes.*

In Papers III and V, the commercial CNC from Celluforce was used as a starting material and in this case the modified CNC (Paper V) did not show any increase in thermal stability to the unmodified CNC, Table 5. This could be because of the inherent higher thermal stability of the Na^+-neutralized CNC from Celluforce. Figure 19 shows that the composites with unmodified CNC were thermally more stable (270 °C) than those reinforced with compared the modified CNC (240 °C) (Paper V). The discoloration of the EAA7 samples (Figure 10 in section 4.2.1) with the modified CNC could again be related to the carboxylate groups of the EAA7 matrix leading to the initiation of degradation.

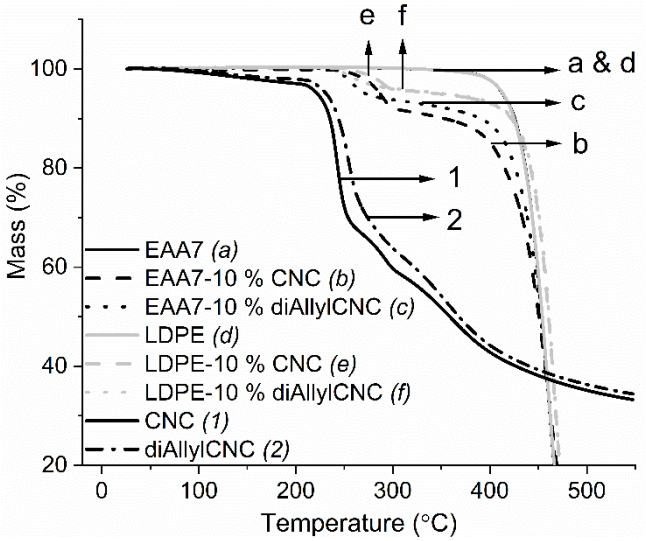

Figure 19: *Thermogravimetric curves showing the thermal degradation of the neat CNC´s, unmodified and modified, the neat polymer matrices and the injection-moulded composites.*

Although previous works have shown that cellulose-based reinforcements can increase or decrease crystallinity, no significant differences in crystallinity or melting point were observed for the composites in this work [26,57,58]. Further details can be found in the appended Papers.

Table 5: *Onset temperature of thermal degradation of the CNC and composites*

Material	Sample designation	T_{onset} (°C)
Matrix (Paper I-V)	EAA	430
	EAA7	430
	LDPE	441
CNC made from MCC (Paper II)	CNC	157
	MorphCNC	224
	diHexylCNC	248
	diAllylCNC	247
CNC from Celluforce	CNC Celluforce	236
	diAllyl CNC (carbonate)	238
	diAllyl CNC (hydroxyazetidinium)	263
(Reference for Paper II) EAA composites with Az-OH modified and unmodified CNC	EAA-10 % CNC	249
	EAA-10 % diAllylCNC	237
	EAA-10 % diAllylCNC	227

(CNC from Celluforce)	(carbonate)	
(Paper II) EAA composites with Az-OH modified and unmodified CNC *(CNC from MCC)* Wet mixing + Compression moulding	EAA-10 % CNC	248
	EAA-10 % MorphCNC	224
	EAA-10 % diHexylCNC	248
	EAA-10 % diAllylCNC	248
	EAA – 10 % diAllyl CNC (Neutralized EAA)	310
(Reference for Paper V) EAA composites with carbonate modified and unmodified CNC *(CNC from Celluforce)*	EAA7-10 % CNC	239
	EAA7-10 % diAllylCNC	239
(Paper V) EAA & LDPE composites with carbonate modified and unmodified CNC *(CNC from Celluforce)* TSE + Injection moulding	EAA7-10 % CNC	265
	EAA7-10 % diAllylCNC	239
	LDPE-10 % CNC	272
	LDPE-10 % diAllylCNC	238

4.3.2 Rheological Properties

The small amplitude oscillatory shear (SAOS) (Papers I, III, V) and steady shear viscosity (Papers I, III, IV, V) were measured, and the rheological properties of the CNF and EAA-CNF suspension were investigated using SAOS and steady shear viscosity experiments which showed an increase in G' and a shear thinning behaviour, explained in detail in the appended papers. Rheological data for the CNC suspensions (modified and unmodified) has been published by Sahlin et.al [44].

Small amplitude oscillatory shear

The strain sweep and frequency sweep data at 150 °C (Paper III) are summarized in Figure 20. The storage modulus (G') of the composites increased with the number of passes due to the breakdown of aggregates, resulting in a better dispersed cellulosic phase with a larger surface area. This led to a better percolated network and a longer relaxation time, seen as a G' plateau in the low frequency region in Figure 10b and as the smaller linear viscoelastic region in Figure 10a [59,60]. The results also show that the S1 screw configuration (longer residence time and higher mixing effect) led to a better composite with a larger G' and a lower slope over the entire frequency range. However, no difference in the magnitude of G' was observed, above a single pass, for the CNF-S1 samples shaped using either the

Maillefer (B) or Maddock (M) type barrier screw, indicating that the shaping screw profile had little effect on the rheological properties of the composites at higher passes (The G' values of CNF-3P-S1-B and CNF-3P-S1-M overlapped, as seen in Figure 11 of Paper III). The figures clearly show that the CNF-based composites have a higher G' and a better percolated network than the CNC-based composites probably due to the difference in aspect ratio.

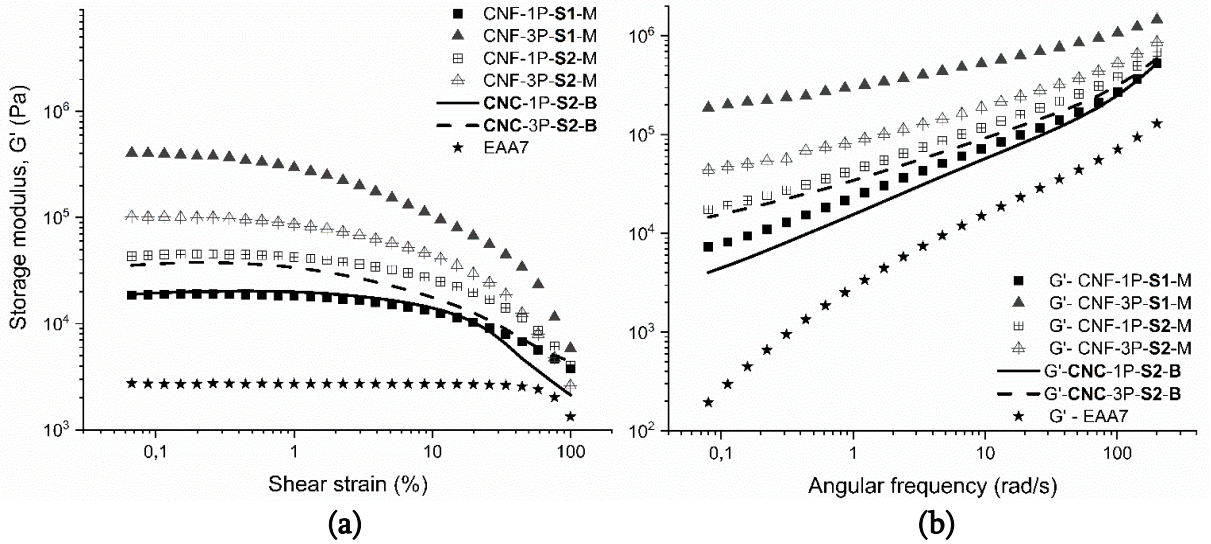

Figure 20: *The storage modulus (G') as functions of* ***(a)*** *the shear strain amplitude and* ***(b)*** *the angular frequency for EAA7 composites reinforced with 20 vol% of CNF (symbols) and CNC (lines) and compounded using S1 (solid symbols) or S2 (open symbols and lines) screw configurations and shaped using either the Maddock type (symbols) or the Maillefer barrier screw (lines).*

When the injection-moulded samples were subjected to an oscillatory strain sweep, Figure 21a, the EAA7-CNC reinforced samples exhibited an overshoot where the G' increased to a certain critical strain after which it decreased. This type of behaviour has been observed in polymer systems where the structural network resists deformation up to a critical strain [61,62]. The LDPE-based samples showed no overshoot and had a G' lower than that of the matrix, the LDPE reinforced with unmodified CNC having the lowest value. The frequency sweep, see Figure 21b, showed the presence of a low frequency plateau with the unmodified CNC, the reinforced CNC having a G' higher than its modified counterpart. At lower frequencies, G'>G'' for the EAA7-10 % CNC samples while G'=G'' for the EAA7 samples reinforced with modified CNC. A percolated network (denoted by the low frequency plateau) was seen only with the EAA7 samples and the strength of the network was emphasised by the mechanical properties, see section 4.3.3.

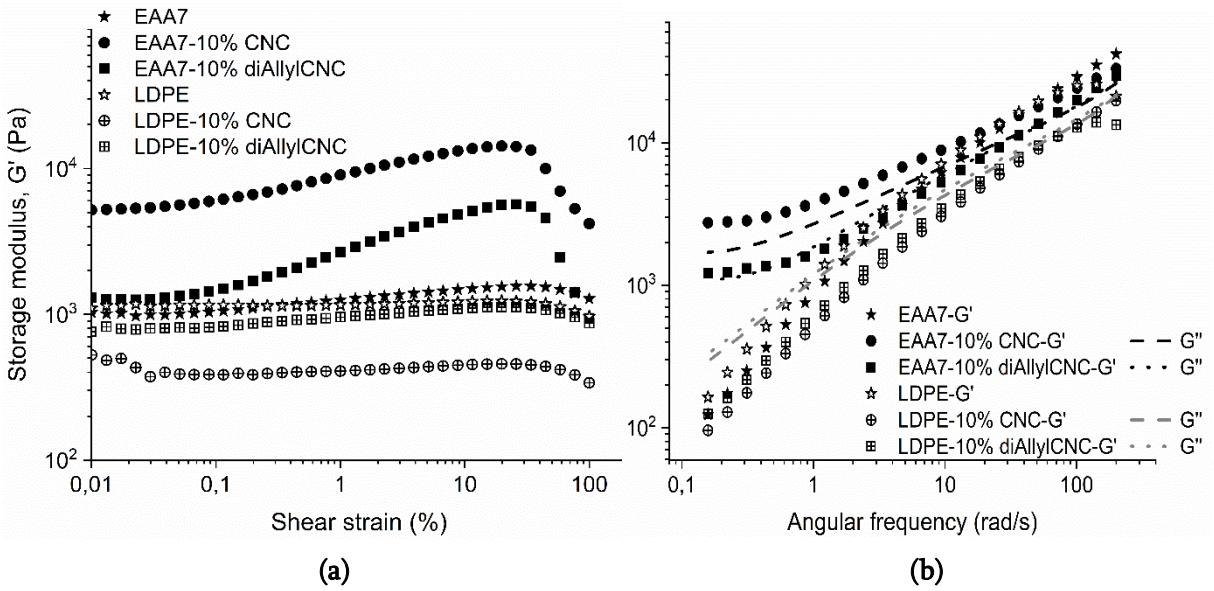

Figure 21: *The storage modulus (G') and loss modulus (G") as functions of* ***(a)*** *shear strain amplitude and* ***(b)*** *angular frequency for EAA7 (filled symbols) and LDPE (unfilled symbols) composites reinforced with unmodified and modified CNC.*

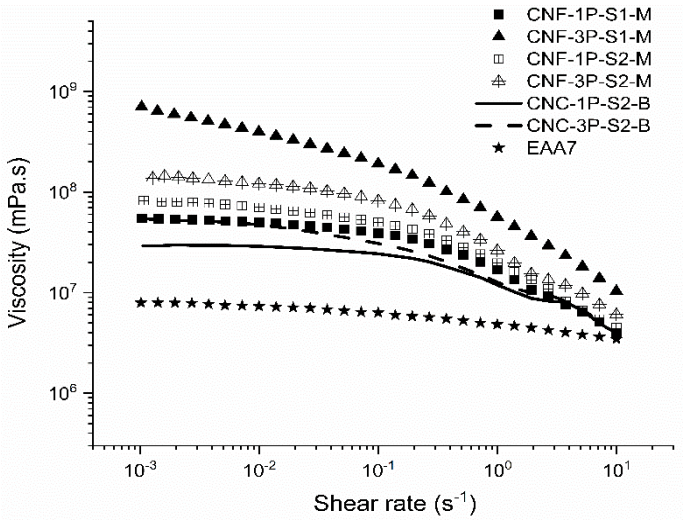

Figure 22: *The viscosity as function of shear rate for EAA7 samples with 20 vol%* ***(a)*** *CNF-containing (symbols) and CNC-containing (lines) composites compounded using S1 (solid symbols) or S2 (open symbols and lines) screw configurations and shaped using either the Maddock (symbols) or the Maillefer type barrier screw (lines).*

Steady Shear

The steady shear viscosity of the composites was investigated at 150 °C in Paper III up to shear rates of 10 s^{-1}, due to the torque limitations. Shear thinning was observed, and the results followed a trend similar to that seen in the SAOS measurements. The viscosity increased with increasing number of passes and the CNF-based samples compounded with

the S1 screw showed the highest viscosity. The viscosity was similar, above a single pass, for the CNF-S1 samples shaped using either the Maillefer (B) or Maddock (M) type barrier screws. The CNC-based samples, on the other hand, showed the presence of a plateau at shear rates of ca. 1-3 s^{-1}, Figure 22. The plateau could be due to a resistance to shear in highly filled composites where the orientation during shear thinning causes a resistance to flow due to clustering [63].

The viscosity was also measured at low shear rate range at 170 °C in Paper IV to investigate the effect of lubricants on compression-moulded EAA samples with 30 wt% TMP or DP, Figure 23. As expected, the filled samples had a higher viscosity and a shear thinning behavior but the samples with lubricants (1.5 wt.%) had a viscosity higher than that of the unlubricated samples.

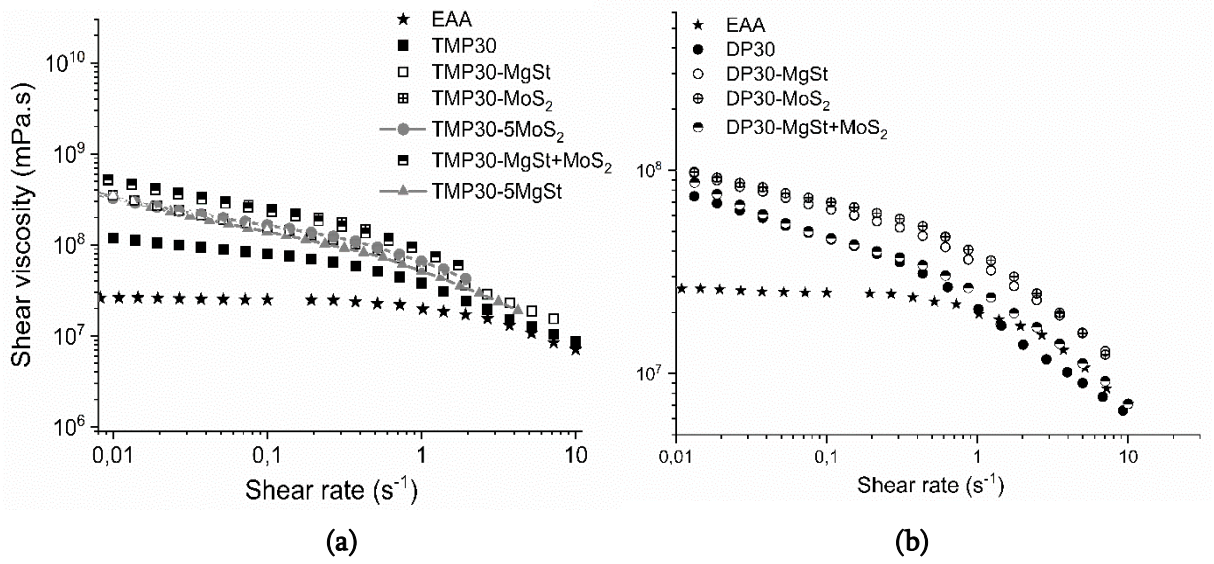

Figure 23: *The viscosity as a function of shear rate for* ***(a)*** *30 wt% TMP and* ***(b)*** *30 wt% DP samples with and without lubricants.*

This increase in melt viscosity for the sample containing lubricants could be due to an improved interaction between the fibers and the matrix as observed in composites where the lubricants tend to behave as compatibilizers at low concentrations [64,65]. The increase in viscosity was greater for the 30 wt% TMP reinforced samples with MoS_2 at low shear rates, the reason being that MoS_2 can interact with the aromatic structure of the lignin present on the TMP [55]. When the lubricant content was increased to 5 wt% in the TMP30 composite, the MoS_2 containing samples showed a slight reduction in viscosity at a concentration of 5 wt%, Figure 23a, and acted both as a compatibilizer and a lubricant. This reinforces the assumption that MoS_2 interacts strongly with the lignin in TMP and that excess MoS_2 which does not interact with the lignin provides a lubricating effect.

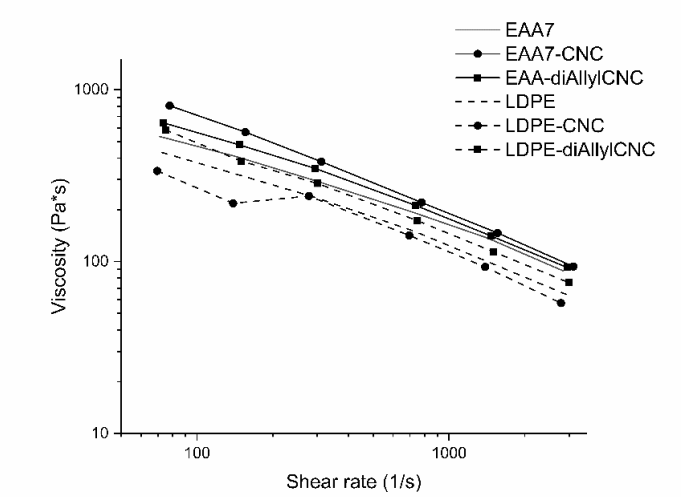

Figure 24: *The shear viscosity of the CNC-composite melts as a function of shear rate after applying Bagley and Rabinowitch corrections*

In Paper V, the shear viscosity of the EAA7 and LDPE composites melts with CNC was measured at high shear rates, corresponding to 58 - 2300 s^{-1}, at 170 °C, as shown in Figure 24. The shear viscosities exhibited a shear thinning behaviour and the EAA7-based melts exhibited a higher viscosity than LDPE based-melts. The addition of CNC to the EAA7 melt resulted in an increase in viscosity at a given shear rate, and the melt containing surface grafted CNC showed a slightly lower viscosity than the melt containing untreated CNC. It is suggested that this may be due to a plasticizing effect of the surface treatment and a less developed filler network. The viscosities of the LDPE-based melts were similar, but the melt containing the surface-treated nanocellulose had the highest viscosity.

4.3.3 Tensile properties

In order to understand the influence of the type of processing method, the processing parameters, the screw design and reinforcement on the tensile mechanical properties of nanocellulose/pulp reinforced thermoplastic composites, a total of 72 sample variants were tested, but due to the differences in loading contents and processing techniques used to produce the samples, not all are comparable. The Young's Modulus (E), yield stress (σ_y), ultimate tensile strength (σ_b) and elongation at break (ε_b) data are presented in Table 6. In Papers I, II and IV, all the composites were prepared via dispersion mixing and compression moulding and, although the cellulose types and loading contents differed, they can be discussed together. EAA containing 15 % acrylic acid was used as the matrix and Table 6 shows that the stiffness and strength of the matrix increased considerably with increasing concentration of the cellulose reinforcement.

Table 6: *Tensile mechanical properties of the composite materials, with different reinforcements, loading contents, matrices and processing techniques with standard deviations in parentheses*

CNF and pulp-based samples					
Type of reinforcement/ Processing method/ Cellulose content	*Sample name*	*Young's modulus* ***(GPa)***	*Yield stress (MPa)*	*Ultimate tensile strength (MPa)*	*Elongation at break (%)*
CNF and pulp Dispersion-mixed, air-dried and compression moulded **(Paper I)** *CNF content = 10 - 70* ***vol%*** *Pulp content = 20, 50 ,70* ***vol%***	EAA	0.3(0.1)	-	24 (1)	491 (19)
	EAA-CNF-10	0.7 (0.1)	-	26 (1)	32 (5)
	EAA-CNF-20	1.6 (0.1)	-	37 (1)	14 (2)
	EAA-CNF-30	3 (0.4)	-	57 (1)	8 (1)
	EAA-CNF-40	4 (0.6)	-	64 (12)	8 (2)
	EAA-CNF-50	4.3 (0.3)	-	65 (5)	6 (1)
	EAA-CNF-60	5.3 (0.6)	-	71 (11)	5 (2)
	EAA-CNF-70	6.2 (0.3)	-	83 (10)	8 (1)
	EAA-Pulp-20	1.8 (0.5)	-	35 (3)	6 (1)
	EAA-Pulp-50	4.4 (1.2)	-	46 (5)	3 (1)
	EAA-Pulp-70	4.9 (0.2)	-	55 (4)	3 (0.3)
TMP or DP, Dispersion-mixed with lubricants, air-dried and compression moulded **(Paper IV)** *Pulp content = 30, 50, 70* ***wt%***	EAA	0.3(0.1)	-	25 (1)	480 (16)
	TMP30	1.4 (0.1)	-	28 (2)	4 (1)
	TMP30-MgSt	1.5 (0.1)	-	35 (2)	5 (1)
	TMP30-MoS_2	1,2 (0.1)	-	33 (1)	6 (1)
	TMP30-MgSt+ MoS_2	1.2 (0.1)	-	33 (3)	5 (3)
	TMP30-5MgSt	1.4 (0.1)	-	32 (3)	4 (0.1)
	TMP30-5MoS_2	1.6 (0.1)	-	39 (1)	5 (0.1)
	TMP30-2.5(MgSt+MoS_2)	1.3 (0.1)	-	27 (3)	3 (0.4)
	TMP50	2.2 (0.03)	-	38 (1)	3 (1)
	TMP50-MgSt	1.7 (0.08)	-	30 (5)	3 (1)
	TMP50-MoS_2	1.8 (0.3)	-	29 (3)	3 (1)
	TMP50-MgSt+ MoS_2	1.6 (0.3)	-	27 (4)	3 (1)
	TMP70	2.4 (0.4)	-	33 (11)	3 (1)
	TMP70-MgSt	2.9 (0.4)	-	32 (6)	2 (1)
	TMP70-MoS_2	3.1 (0.1)	-	31 (6)	3 (1)
	DP30	0.6 (0.06)	-	22 (1)	12 (1)
	DP30-MgSt	0.6 (0.03)	-	22 (1)	12 (1)
	DP30-MoS_2	0.5 (0.02)	-	18 (1)	23 (2)
	DP30-MgSt+MoS_2	0.8 (0.1)	-	28 (5)	13 (3)
	DP50	1.2 (0.06)	-	39 (3)	10 (1)
	DP50-MgSt	1.3 (0.2)	-	36 (3)	7 (1)
	DP50-MoS_2	1.0 (0.07)	-	32 (1)	11 (1)
	DP50-MgSt+ MoS_2	1.3 (0.2)	-	41 (4)	7 (1)
	DP70	1.9 (0.1)	-	48 (4)	5 (1)
	DP70-MgSt	2.3 (0.2)	-	35 (1)	5 (1)

	DP70-MoS_2	2.0 (0.1)	-	43 (4)	6 (1)

CNF and CNC-based samples

Type of reinforcement/ Processing method/ Cellulose content	*Sample name*	*Young's modulus* ***(MPa)***	*Yield stress (MPa)*	*Ultimate tensile strength (MPa)*	*Elongation at break (%)*
CNC from MCC, Az modified, Dispersion-mixed, air-dried and compression moulded **(Paper II)** *CNC content = 0.1, 1, 10 wt%*	EAA	322 (5)	15.1 (0.6)	25.8 (1.2)	255 (6)
	EAA-0.1% CNC	270 (13)	13.5 (0.3)	24.5 (0.7)	278 (6)
	EAA-0.1% MorphCNC	294 (28)	14.1 (0.5)	24.3 (0.8)	284 (11)
	EAA-0.1% diAllylCNC	237 (25)	12.1 (1.0)	21.2 (1.3)	276 (11)
	EAA-0.1% diHexylCNC	249 (24)	12.8 (0.6)	23.5 (1.4)	288 (15)
	EAA-1% CNC	353 (18)	15.3 (0.5)	25.3 (1.7)	246 (7)
	EAA-1% MorphCNC	367 (22)	15.2 (0.6)	23.4 (1.3)	252 (10)
	EAA-1% diAllylCNC	314 (21)	14.1 (0.6)	22.9 (1.0)	261 (10)
	EAA-1% diHexylCNC	295 (16)	14.1 (0.4)	23.7 (1.2)	267 (10)
	EAA-10% CNC	921 (64)	-	21.9 (0.9)	6 (1)
	EAA-10% MorphCNC	678 (46)	15.1 (0.4)	14.2 (2.3)	11 (10)
	EAA-10% diAllylCNC	864 (32)	21.1 (0.7)	19.7 (0.8)	31 (22)
	EAA-10% diHexylCNC	678 (21)	17.9 (0.4)	16.5 (1.0)	28 (15)
CelluForce CNC, Az modified produced as in Paper II ***(Reference)*** *CNC content = 10* ***wt%*** *CNF content = 20* ***vol%***	EAA7-10% CNC	860 (21)	-	18 (0.4)	88 (20)
	EAA7-10% diAllylCNC	783 (27)	-	16 (0.3)	58 (8)
	EAA-10% CNC	948 (35)	-	23 (0.2)	8 (0.7)
	EAA-10% diAllylCNC	697 (17)	16 (0.2)	22 (1)	206 (18)
	EAA-10% diAllylCNC (Carbonate modified)	544 (14)	14 (0.2)	17 (2)	115 (43)
	EAA7-CNF-20*	2270 (380)	-	56 (2)	10.7 (1.23)
CNF and Celluforce CNC Dispersion-mixed master-batch, air-dried, Compounded with EAA7 matrix and single-screw extruded **(Paper III)** *CNF content = 20* ***vol%*** *CNC content = 20* ***vol%***	EAA7	148 (10)	-	19 (3)	442 (70)
	CNF-1P-S1-M	550 (80)	-	10.3 (2)	7 (2)
	CNF-2P-S1-M	950 (70)	-	26 (1)	10 (1)
	CNF-3P-S1-M	1340 (170)	-	28 (1)	10 (1)
	CNF-1P-S2-M	470 (50)	-	10.6 (1)	10 (1)
	CNF-2P-S2-M	510 (50)	-	13.5 (1)	11 (2)
	CNF-3P-S2-M	510 (40)	-	15 (1)	12.5 (1)
	CNF-1P-S1-B	750 (50)	-	12.5 (2)	8 (1)
	CNF-2P-S1-B	1534 (110)	-	28 (1.5)	8 (2)
	CNF-3P-S1-B	1520 (160)	-	30.5 (2)	8 (1)
	CNC-1P-S2-B	400 (20)	-	12.5 (0.3)	47 (4)
	CNC-2P-S2-B	500 (80)	-	15.5 (1)	55 (5)
	CNC-3P-S2-B	600 (70)	-	16 (0.5)	62 (3)
CelluForce CNC, Carbonate modified	EAA7	109 (2)	5.7 (0.1)	16.8 (0.6)	90.6 (2.6)
	EAA7-10 % CNC	197 (14)	12.9 (0.3)	17.5 (0.3)	36.7 (3.6)

Water-assisted extrusion in TSE and injection moulded **(Paper V)** *CNC content = 10* ***wt%***	EAA7-10 % diAllylCNC	166 (4)	8 (0.2)	16 (0.5)	59 (3.2)
	LDPE	150 (7)	7 (0.1)	13 (0.3)	62 (3.6)
	LDPE-10 % CNC	210 (2)	8.5 (0.3)	12.1 (0.3)	39.4 (1)
	LDPE-10 % diAllylCNC	209 (6)	9 (0.2)	12.6 (0.1)	38 (2.1)

***** Dispersion mixed and compression-moulded reference sample with composition similar to Paper III

In Paper I, at a cellulose concentration of 70 vol%, the stiffness and strength of the composite increased by factors of 21 and 3.5, respectively, for the CNF-based and 16 and 2.3 for the pulp-based composites. Up to 70 vol% the CNF composites showed an increase in the tensile properties with a critical threshold concentration of 20-30 vol%, which has also been observed in other works [29,58]. This concentration coincided with both the region where the Cox-Krenchel model underestimated the stiffness increase of the composites, Figure 25b, and with the peak effective stiffness ($E_{f,1}$), as discussed in Paper I. Below the critical concentration threshold, the stiffness and strength were similar to those of the pulp-based composites suggesting that this concentration was related to the mechanical percolation of the system, where entanglements between the reinforcement can enhance the stiffness and strength of the composites [29,58]. The variation in stiffness between pulp and CNF-based composites was negligible up to 50 vol% but a difference in strength was clearly observed, above 20 vol%, the CNF being stronger, probably due to an increased surface area and a better stress transfer, see Table 6 and Figure 25(a).

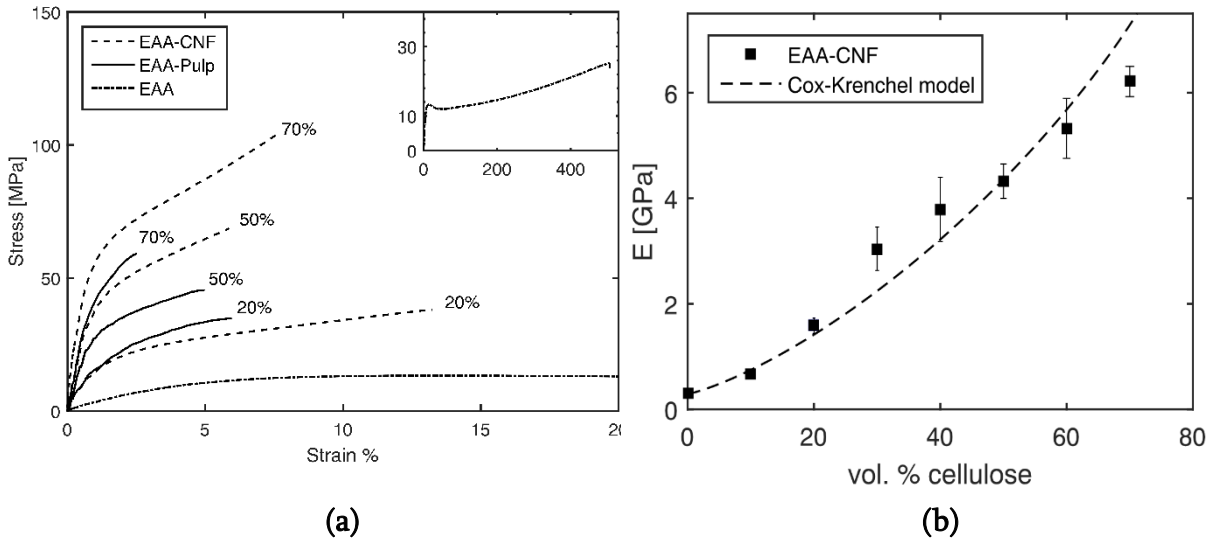

Figure 25: ***(a)*** *Typical stress-strain curves of CNF–EAA and pulp–EAA composites (inset shows the full stress–strain behavior for EAA and* ***(b)*** *Elastic modulus along with the Cox–Krenchel prediction for a CNF–EAA composites.*

In Paper II, the composites contained 0.1, 1 and 10 wt% CNC, but only the 10 wt% composite is discussed here since the change in mechanical properties was more evident at this concentration, Table 6. The effects of CNC at lower concentrations can be found in

Paper II. Compared to the matrix, the unmodified and the diAllyl-modified CNC reinforced composites showed an increase in the modulus by factors of 2.9 and 2.7, respectively, but the main effect of the modified CNC was observed in the elongation and yield stress which were respectively 31 % and 21.1 MPa for the diAllyl-CNC, but only 6 % with no yield behavior in the case of the unmodified CNC. All the modified CNC composites had a combination of high modulus, high yield stress and high elongation with diAllyl being the highest, Table 6, probably because improved interactions led to a more ductile interphase as discussed in Paper II.

In Paper IV, composites containing thermomechanical (TMP) and dissolving (DP) pulp had lubricants, magnesium stearate (MgSt) and molybdenum disulphide (MoS_2), added. These DP-containing and TMP-containing composites, at 70 wt% fiber content, showed an increase in tensile modulus by factors of 6.3 and 8.1, respectively without lubricants, and by factors of 8 and 10.7, respectively with lubricants. The addition of a lubricant was beneficial for the mechanical properties of the TMP-based samples at lower loadings, 30 wt%, where the mechanical properties suggested a behaviour similar to that of a compatibilizer especially with MoS_2 even at high lubricant concentration (5 wt% in the TMP30 composites) [64,65]. Their effect on the strength of the DP-based samples was however poor, unless they were added in combination. Interestingly, some DP-based samples containing MoS_2 did show a significantly greater elongation-at-break, the details of which are discussed in the appended papers.

In case of the EAA7 composite prepared by melt mixing in Papers III and V, the mechanical properties increased much less than those of the compression-moulded samples. In Paper III, the 20 vol% samples prepared by compounding a master-batch with EAA7, had a modulus which improved by a factor of 4.8. The mechanical properties (modulus, strength-at-break and elongation-at-break) increased with increasing number of passes, despite the discoloration/degradation and hence only the three-pass composites are discussed here. The properties of the other samples at lower passes are shown in Table 6. In the case of the CNF-reinforced composites compounded at 100 rpm using the S1 screw configuration and shaped using the Maddock type barrier screw (CNF-3P-S1-M), the longer residence time led to improved mechanical properties because of the better mixing and greater break down of aggregates than in the samples compounded using the S2 screw configuration (CNF-3P-S2-M), which had a shorter residence time, Table 6. The mechanical properties were also influenced by the screw type selected during shaping and this was seen when the CNF pellets (compounded using S1 screw) were shaped with the Maillefer type barrier screw (CNF-3P-S1-B) to exhibit the best properties, with tensile modulus (E), stress-at-break (σ_b) and elongation at break (ε_b) values of 1530 MPa, 30.4 MPa and 9.6 %, respectively, Table 6. The combination of the S1 screw configuration during compounding and the Maillefer barrier screw during shaping gave the highest mechanical properties of all the extruded

composites, probably because a better dispersive and distributive mixing was achieved with this combination. If the favourable choice of screw is are made for compounding and shaping, the CNC samples (*CNC-S2-B* series) can also have reinforcing capabilities better than or similar to those of the CNF reinforced sample (*CNF-S2-M* series), as shown in Figure 26.

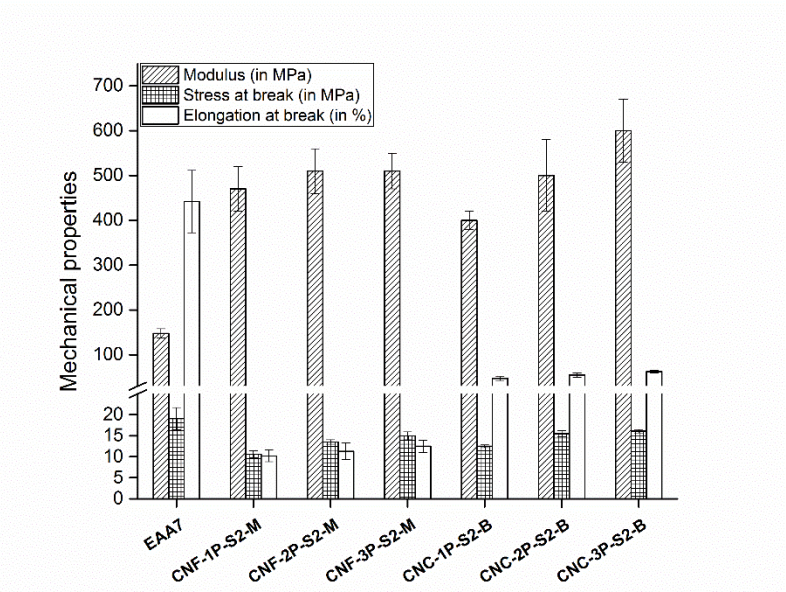

Figure 26: *The mechanical properties of CNF- and CNC-reinforced samples compounded using the S2 screw design and shaped with the Maddock type barrier screw (CNF) and Maillefer barrier screw (CNC).*

In Paper V, EAA7 and LDPE were used as matrices to produce 10 wt.% CNC reinforced composites by using water-assisted extrusion and injection moulding (upscaling from Paper II). However, as in Paper III, the increase in mechanical properties was lower. The stiffness of the EAA7 and LDPE composites with unmodified CNC increased by factors of 1.4 and 1.8, respectively. With the LDPE as matrix, the modified and unmodified-CNC-based samples behaved similarly, with little difference between the stiffnesses and strengths of the composites. The better properties of the EAA7 composites containing unmodified CNC may indicate the influence of processing on the interaction between the matrix and the reinforcing element. In all these cases, the addition of CNC had little effect on the ultimate tensile strength, but the addition of the nanocrystals lowered the elongation-at-break as discussed in Paper V

The melt processing technique used played a role for the final properties of the composites, shown in Figure 27, and to study the extent to which the melt flow influences the mechanical properties of the composites reference samples were produced using an aqueous dispersion of EAA7 reinforced with CNF (reference as in Paper III) and CNC from CelluForce and surface modified using both hydroxyazetidinium salts and a carbonate reagent. These samples were dispersion-mixed, air-dried and compression-moulded as

reported in Papers I and II. As can be seen in Table 6, the stiffness of the CelluForce-CNC with EAA7 as matrix increased significantly but the ultimate tensile strength showed no difference. Furthermore, the EAA samples with Celluforce CNC showed stiffness and strength values similar to those of the compression-moulded samples in Paper II, suggesting that the choice of CNC grade did not influence the stiffness of the material significantly. In the case of the EAA7-CNF-20 (reference to the CNF materials in Paper III), a large difference in the mechanical properties was however observed, see Figure 27.

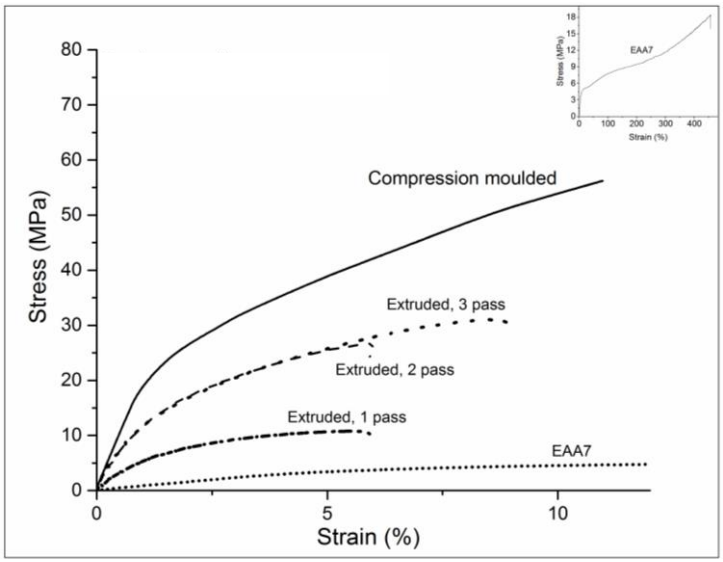

Figure 27: *Comparison of the mechanical properties of extruded 20 vol% CNF reinforced sample produced in Paper III (CNF-S1-B series) with a reference compression-moulded sample with same composition prepared via dispersion mixing (EAA7-CNF-20*).*

4.3.4 Dynamic mechanical analysis

In Paper I, the dynamic storage modulus (E') and mechanical loss factor (tan δ) of the EAA-CNF composites were determined over a range of temperatures as shown in figure 28. The addition of CNF increased the storage modulus (E') throughout the temperature range and three transition peaks were identified up to a CNF concentration of 30 vol%. The addition of CNF led to a general stiffening effect, resulting in the melting peaks becoming less pronounced above 40 vol%.

In Papers II, IV and V, the variation in the slope of the tan δ versus strain amplitude curve for the matrix and other samples was determined to extract qualitative information about the interphase between the matrix and the reinforcement [27,66,67]. The tan δ was measured as a function of amplitude of the sinusoidal deformation at room temperature for (a) the dispersion-mixed and compression-moulded composites with 10 wt.% CNC, (b) the dispersion-mixed and compression-moulded TMP and DP reinforced composites with

lubricants and (c) the water-assisted extruded and injection-moulded composites with 10 wt.% CNC, in comparison with the neat matrices.

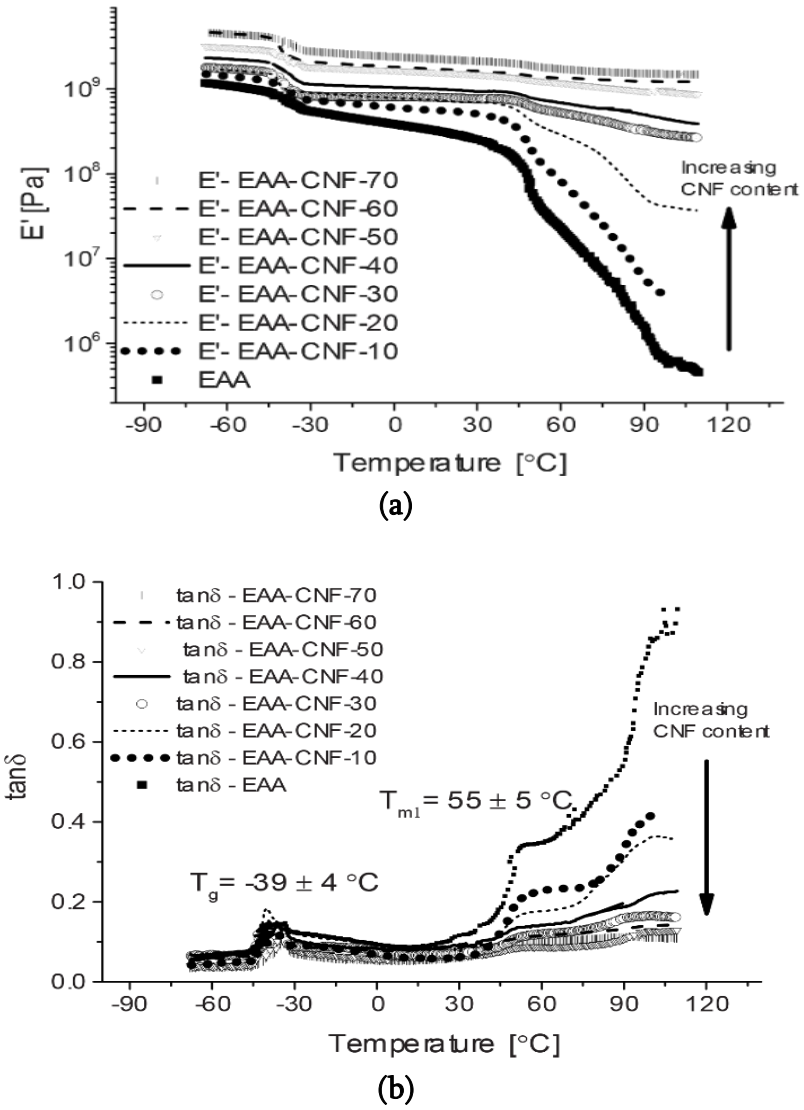

Figure 28: ***(a)*** *Storage modulus (E') and* ***(b)*** *loss factor (tan δ) of CNF-EAA composites measured at a constant strain amplitude at temperature from -80 to 110 °C.*

In Papers II and V, the surface grafting clearly affected the behaviour of the loss factor over the whole strain amplitude range, Figure 29, where the surface modification with di Allyl had a slope similar to that of the matrix and was less sensitive to the increasing strain amplitude. In Figure 29b, EAA7-based samples containing unmodified and modified CNC exhibited a plateau in loss factor curve at low strain amplitudes, but with increasing strain amplitude, the slope of the loss factor increased for the EAA7 with the unmodified CNC. This suggests that the surface treatment created a more stable interphase region in this case and to some extent supported the hypothesis put forward in Paper II regarding the greater

extensibility of the composite, Table 6. With LDPE as the matrix, the changes in loss factor were small, as discussed in Paper V.

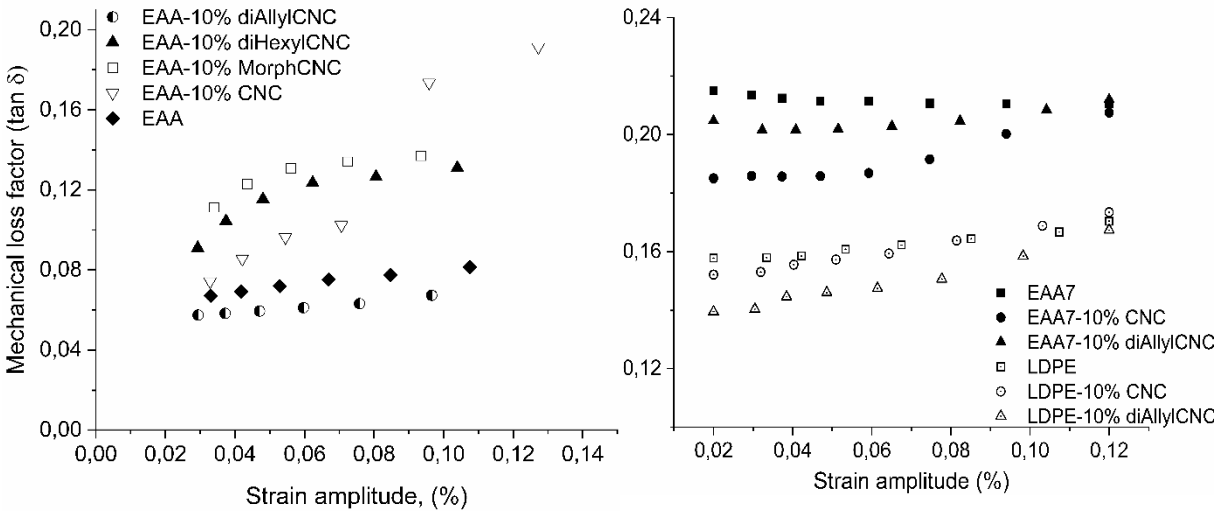

Figure 29: *The mechanical loss factor as a function of the applied strain amplitude for 10 wt% modified or unmodified CNC reinforced* ***(a)*** *compression-moulded EAA composites and* ***(b)*** *injection-moulded EAA7 and LDPE composites.*

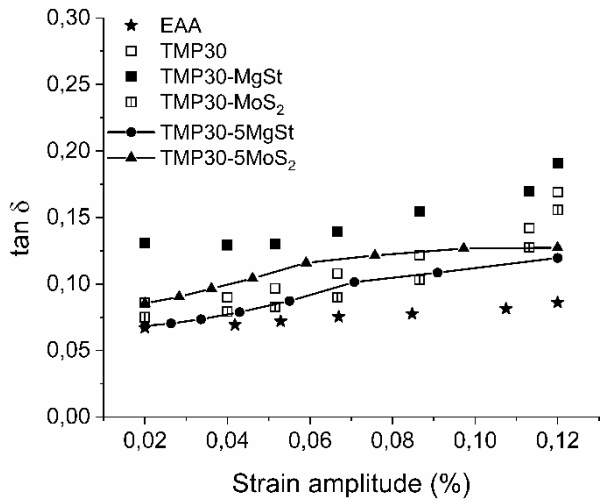

Figure 30: *The mechanical loss factor as a function of applied strain amplitude for 30 wt% TMP samples containing different amounts of MoS_2 and MgSt.*

The addition of a lubricant showed a behaviour similar to that of a compatibilizer, particularly at the low loading content of 30 wt% in the TMP30 samples with MoS_2 as shown in Figure 30. When the MoS_2 concentration was increased, a plateau was observed at higher strain amplitudes which was not present in the TMP30 composite with 1.5 wt% MoS_2 . The relatively more stable interphase correlated with the increase in mechanical properties, Table 6, but the effect on the DP-based samples was more effective when MoS_2 and MgSt were added as a combination, as discussed in detail in Paper IV.

5 CONCLUSIONS

The addition of a cellulose reinforcement to the thermoplastics studied improved their mechanical properties regardless of the aspect ratio of the reinforcement, but the magnitude of the improvement was largely dependent on the type of melt-processing technique that was used. In case of the compression-moulded samples, the stiffness of the composite was increased by a factor of 0.8 to 21 depending on the type of reinforcement used and on the loading content. On the other hand, the increase in stiffness obtained as a result of processing methods involving high shear rates such as extrusion and injection moulding was much lower, the increase being by a factor of 1.8 – 10. The difference in properties was related to the aggregates created during continuous melt processing, unlike the well-dispersed compression-moulded samples.

In large-scale processing, it was shown that multiple re-extrusions could breakdown the aggregates and improve the strength of the percolated cellulose network to achieve optimum properties in the composites. Even though the nanocellulose showed discoloration due to repeated extrusion and exposure to high temperatures, the stiffness and strength were not reduced. In this case, two-passes or a re-extrusion were found to improve the properties and homogeneity of the composite. To minimize the formation of aggregates and improve dispersion, water-assisted mixing methods were found to be beneficial on both a small and large scale. On the large scale, the tensile strength of a composite produced by wet mixing of 10 wt% unmodified CNC was greater than that of the samples produced by dry mixing of the CNC reinforcement at 28 wt%. The wet-mixed samples also showed a strength similar to that of the compression-moulded samples at a loading content of 10 wt%, despite the great differences in stiffness.

Apart from the upscaling of the modified CNC production and subsequent water-assisted extrusion to obtain composites, emphasis was also placed on highlighting the importance of the screw configuration, the type of screw, the number of passes and the morphology of reinforcement in controlling the final properties of nanocellulose-based composites. In the processing of cellulose-composites, the combination of dispersive and distributive mixing was most important for obtaining the optimum properties, rather than either of them alone. In addition, the water-assisted mixing methods were an efficient way to introduce lubricants in the system. The lubricant system and concentration should be selected based on their concentration and reinforcement composition as they can decide whether it behaved like a compatibilizer and/or lubricant. Depending on the type of CNC used, the surface modification had an influence on the interphase of the composite by improving its thermal properties and toughness, but the extent of their effectiveness was dependent on certain factors in the system (pH or type of functional groups).

6 FUTURE WORK

Based on the findings from the current work, it would be interesting to explore:

- the effect of high shear rates on the properties of surface-modified cellulose to show the effectiveness of the modification after exposure to high shear forces and extensional forces during compounding and shaping.

- the effect of orientation of the cellulose reinforcements on the strength of the percolated cellulose network, as the strength of a cellulose composite is determined not only by the adhesion between the fiber and the matrix but also by the strength of the cellulose network itself.

- the use as reinforcements of pulps with different hemicellulose or lignin concentrations and of a modified pulp which could fibrillate during melt processing.

- Since a polymer composite tends to have two or more components, it would be interesting to study end of life cycle recycling and the impact of re-extrusion on thermal degradation/durability.

7 ACKNOWLEDGEMENT

I would like to express my sincere gratitude and thanks to my supervisor Antal Boldizar for his support, time, patience and guidance. I will always appreciate all the advice and help that I have received in the discussions with you and special thanks also for your encouragement and support for my extra-curricular activities. I would also like to thank Mikael Rigdahl for all the discussions and help with the manuscripts. You were really patient and went above and beyond to help me with my work which I will always be grateful for.

The Swedish Foundation for Strategic Research is gratefully acknowledged for its financial support for this project. Borregaard, Jan Wahlberg at Tetrapak, Karl Banke, Anette Munch Elmer and Patrick from Polykemi are specially thanked for cooperation, patience and assistance during the large-scale trials, especially during this pandemic. Dr. Anthony Bristow is gratefully acknowledged for the linguistic revision of the manuscript.

My thanks also to Roland Kadar and Giada Lo Re for the discussions and support during these years, I have thoroughly enjoyed every moment of it. Håkan Millqvist and Roger Sagdahl are thanked for their constant support in the lab. I would like to extend special thanks to Johannes Thunberg and Kristina Karlsson for all the support and advice that they have given me. You both have been friends as well as mentors. I would like to acknowledge my co-authors and colleagues from the Department of Chemistry and Chemical Engineering. Thank you for all the energy and time you have put into these works and also thank you for explaining the chemistry-related topics, especially Anna Peterson and Karin Sahlin for having the patience to discuss with me no matter how trivial and repetitive my questions were.

Lars Hammar and Jörgen Romild are thanked for their experimental support. The colleagues at the Department of Industrial and Materials Science are thanked for the best possible atmosphere and special thanks to my office mate for keeping the mood jovial and bearing with me. All the members of the polymer group are thanked for their unending support (thank you for covering for me) and helping me out whenever I was lost. Thank you, Lilian, for helping me be organized and supporting me all these years. Angelica, Ezgi, Bashar and Sylvia, I hope to work more with you all in the future. It has truly been a pleasure.

Finally, I would like to thank my upgraded family, Appaji, Mami and Dwivarna, for all the support and love. A special thanks to my wife who is an inspiration to me, and no amount of words are enough to express how much you mean to me. My parents, without whom I would never have gotten here- thank you for the blessings and unwavering love and support. To my siblings - my precious angels, without you both everything would be boring and incomplete. **HSVJ!**

8 REFERENCES

[1] K.L. Yam, B.K. Gogoi, C.C. Lai, S.E. Selke, Composites from compounding wood fibers with recycled high density polyethylene, Polym. Eng. Sci. 30 (1990) 693–699. https://doi.org/10.1002/pen.760301109.

[2] N.M. Stark, R.E. Rowlands, Effects of wood fiber characteristics on mechanical properties of wood/polypropylene composites, Wood Fiber Sci. 35 (2003) 167–174.

[3] T. Saito, S. Kimura, Y. Nishiyama, A. Isogai, Cellulose Nanofibers Prepared by TEMPO-Mediated Oxidation of Native Cellulose, Biomacromolecules. 8 (2007) 2485–2491. https://doi.org/10.1021/bm0703970.

[4] L. Wågberg, G. Decher, M. Norgren, T. Lindström, M. Ankerfors, K. Axnäs, The build-up of polyelectrolyte multilayers of microfibrillated cellulose and cationic polyelectrolytes, Langmuir. 24 (2008) 784–795. https://doi.org/10.1021/la702481v.

[5] M. Pääkko, M. Ankerfors, H. Kosonen, A. Nykänen, S. Ahola, M. Österberg, J. Ruokolainen, J. Laine, P.T. Larsson, O. Ikkala, T. Lindström, Enzymatic hydrolysis combined with mechanical shearing and high-pressure homogenization for nanoscale cellulose fibrils and strong gels, Biomacromolecules. 8 (2007) 1934–1941. https://doi.org/10.1021/bm061215p.

[6] L.A. Berglund, T. Peijs, Cellulose Biocomposites—From Bulk Moldings to Nanostructured Systems, MRS Bull. 35 (2010) 201–207. https://doi.org/10.1557/mrs2010.652.

[7] K. Oksman, Y. Aitomäki, A.P. Mathew, G. Siqueira, Q. Zhou, S. Butylina, S. Tanpichai, X. Zhou, S. Hooshmand, Review of the recent developments in cellulose nanocomposite processing, Compos. Part A Appl. Sci. Manuf. 83 (2016) 2–18. https://doi.org/10.1016/j.compositesa.2015.10.041.

[8] C. Klason, J. Kubát, H.-E. Strömvall, The Efficiency of Cellulosic Fillers in Common Thermoplastics. Part 1. Filling without Processing Aids or Coupling Agents, Int. J. Polym. Mater. Polym. Biomater. 10 (1984) 159–187. https://doi.org/10.1080/00914038408080268.

[9] R.J. Moon, A. Martini, J. Nairn, J. Simonsen, J. Youngblood, Cellulose nanomaterials review: structure, properties and nanocomposites, Chem. Soc. Rev. Chem. Soc. Rev. 40 (2011) 3941–3994. https://doi.org/10.1039/c0cs00108b.

[10] A. Dufresne, Cellulose and Potential reinforcement, in: Nanocellulose From Nat. to High Perform. Tailored Mater., De Gruyter, Berlin, Boston, 2017: pp. 1–42. https://doi.org/10.1515/9783110480412.

[11] R. Passas, Natural fibres for paper and packaging, in: Handb. Nat. Fibres Process. Appl., Elsevier, 2012: pp. 367–400. https://doi.org/10.1533/9780857095510.2.367.

[12] H. Kumar, L.P. Christopher, Recent trends and developments in dissolving pulp production and application, Cellulose. 24 (2017) 2347–2365. https://doi.org/10.1007/s10570-017-1285-y.

[13] D. Klemm, F. Kramer, S. Moritz, T. Lindström, M. Ankerfors, D. Gray, A. Dorris, Nanocelluloses: A new family of nature-based materials, Angew. Chemie - Int. Ed. 50

(2011) 5438–5466. https://doi.org/10.1002/anie.201001273.

[14] A.K. Bharimalla, S.P. Deshmukh, P.G. Patil, N. Vigneshwaran, Energy Efficient Manufacturing of Nanocellulose by Chemo-and Bio-Mechanical Processes: A Review, World J. Nano Sci. Engi-Neering. 5 (2015) 204–212. https://doi.org/10.4236/wjnse.2015.54021.

[15] H.A. Krässig, Cellulose: Structure, accessibility and reactivity, Gordon and Breach Publishers, Philadelphia, 1993. https://doi.org/10.1002/pola.1994.080321221.

[16] H. Kargarzadeh, I. Ahmad, S. Thomas, A. Dufresne, Methods for Extraction of Nanocellulose from Various Sources, in: Alain Dufrsne (Ed.), Handb. Nano-Cellulose Cellul. Nanocomposites, John Wiley & Sons, Incorporated, 2017: pp. 1–50.

[17] Y. Habibi, L.A. Lucia, O.J. Rojas, Cellulose nanocrystals: Chemistry, self-assembly, and applications, Chem. Rev. 110 (2010) 3479–3500. https://doi.org/10.1021/cr900339w.

[18] K.Y. Lee, Y. Aitomäki, L.A. Berglund, K. Oksman, A. Bismarck, On the use of nanocellulose as reinforcement in polymer matrix composites, Compos. Sci. Technol. 105 (2014) 15–27. https://doi.org/10.1016/j.compscitech.2014.08.032.

[19] M. Börjesson, K. Sahlin, D. Bernin, G. Westman, Increased thermal stability of nanocellulose composites by functionalization of the sulfate groups on cellulose nanocrystals with azetidinium ions, J. Appl. Polym. Sci. 135 (2018) 45963. https://doi.org/10.1002/app.45963.

[20] A. Boldizar, C. Klason, J. Kubát, P. Näslund, P. Sáha, Prehydrolyzed Cellulose as Reinforcing Filler for Thermoplastics, Int. J. Polym. Mater. 11 (1987) 229–262. https://doi.org/10.1080/00914038708078665.

[21] K. Berggren, C. Klason, J. Kubat, Spritzgiessen holzmehlhaltiger thermoplaste, Kunststoffe. 65 (1975) 69–74.

[22] R. Ariño, A. Boldizar, Processing and mechanical properties of thermoplastic composites based on cellulose fibers and ethylene-acrylic acid copolymer, Polym. Eng. Sci. 52 (2012) 1951–1957. https://doi.org/10.1002/pen.23134.

[23] L.A. Berglund, T. Peijs, Cellulose Biocomposites—From Bulk Moldings to Nanostructured Systems, MRS Bull. 35 (2010) 201–207. https://doi.org/10.1557/mrs2010.652.

[24] J. Zhang, S. Chen, J. Su, X. Shi, J. Jin, X. Wang, Z. Xu, Non-isothermal crystallization kinetics and melting behavior of EAA with different acrylic acid content, J. Therm. Anal. Calorim. 97 (2009) 959–967. https://doi.org/10.1007/s10973-009-0014-7.

[25] R. Cooper, C. Guy, N. Seung, K. Vredeveld, High Performance Copolymer Dispersions For Flexible Packaging, n.d. https://www.aimcal.org/uploads/4/6/6/9/46695933/guy_abstract.pdf (accessed August 9, 2018).

[26] M.A.S. Azizi Samir, F. Alloin, J.-Y. Sanchez, A. Dufresne, Cellulose nanocrystals reinforced poly(oxyethylene), Polymer (Guildf). 45 (2004) 4149–4157. https://doi.org/10.1016/j.polymer.2004.03.094.

[27] L. Forsgren, K. Sahlin-Sjövold, A. Venkatesh, J. Thunberg, R. Kádár, A. Boldizar, G. Westman, M. Rigdahl, Composites with surface-grafted cellulose nanocrystals (CNC), J.

Mater. Sci. 54 (2019) 3009–3022. https://doi.org/10.1007/s10853-018-3029-2.

[28] T. Zheng, S. Pilla, Melt Processing of Cellulose Nanocrystal-Filled Composites: Toward Reinforcement and Foam Nucleation, Ind. Eng. Chem. Res. 59 (2020) 8511–8531. https://doi.org/10.1021/acs.iecr.0c00170.

[29] K. Larsson, L.A. Berglund, M. Ankerfors, T. Lindström, Polylactide latex/nanofibrillated cellulose bionanocomposites of high nanofibrillated cellulose content and nanopaper network structure prepared by a papermaking route, J. Appl. Polym. Sci. 125 (2012) 2460–2466. https://doi.org/10.1002/app.36413.

[30] J.M.B. Fernandes Diniz, M.H. Gil, J.A.A.M. Castro, Hornification - Its origin and interpretation in wood pulps, Wood Sci. Technol. 37 (2004) 489–494. https://doi.org/10.1007/s00226-003-0216-2.

[31] M. Le Baillif, K. Oksman, The Effect of Processing on Fiber Dispersion, Fiber Length, and Thermal Degradation of Bleached Sulfite Cellulose Fiber Polypropylene Composites, J. Thermoplast. Compos. Mater. 22 (2009) 115–133.

[32] S. Migneault, A. Koubaa, F. Erchiqui, A. Chaala, K. Englund, C. Krause, M. Wolcott, Effect of fiber length on processing and properties of extruded wood-fiber/HDPE composites, J. Appl. Polym. Sci. 110 (2008) 1085–1092. https://doi.org/10.1002/app.28720.

[33] A. Venkatesh, J. Thunberg, K. Sahlin-Sjövold, M. Rigdahl, A. Boldizar, Melt Processing of Ethylene-Acrylic Acid Copolymer Composites Reinforced with Nanocellulose, Polym. Eng. Sci. 60 (2020) 956–967. https://doi.org/10.1002/pen.25351.

[34] N. Herrera, A.P. Mathew, K. Oksman, Plasticized polylactic acid/cellulose nanocomposites prepared using melt-extrusion and liquid feeding: Mechanical, thermal and optical properties, Compos. Sci. Technol. 106 (2015) 149–155. https://doi.org/10.1016/j.compscitech.2014.11.012.

[35] N. Herrera, A.M. Salaberria, A.P. Mathew, K. Oksman, Plasticized polylactic acid nanocomposite films with cellulose and chitin nanocrystals prepared using extrusion and compression molding with two cooling rates: Effects on mechanical, thermal and optical properties, Compos. Part A Appl. Sci. Manuf. (2016). https://doi.org/10.1016/j.compositesa.2015.05.024.

[36] J. Peng, P.J. Walsh, R.C. Sabo, L.-S. Turng, C.M. Clemons, Water-assisted compounding of cellulose nanocrystals into polyamide 6 for use as a nucleating agent for microcellular foaming, Polymer (Guildf). 84 (2016) 158–166. https://doi.org/10.1016/J.POLYMER.2015.12.050.

[37] J. Karger-Kocsis, Á. Kmetty, L. Lendvai, S. Drakopoulos, T. Bárány, Water-Assisted Production of Thermoplastic Nanocomposites: A Review, Materials (Basel). 8 (2014) 72–95. https://doi.org/10.3390/ma8010072.

[38] T.A.T. Yasim-Anuar, H. Ariffin, M.N.F. Norrrahim, M.A. Hassan, Y. Andou, T. Tsukegi, H. Nishida, Well-Dispersed Cellulose Nanofiber in Low Density Polyethylene Nanocomposite by Liquid-Assisted Extrusion, Polymers (Basel). 12 (2020) 927. https://doi.org/10.3390/polym12040927.

[39] A.B. Strong, Plastics: materials and processing, 3rd ed., Pearson Prentice Hall, 2006.

[40] I. Tsiropoulos, A.P.C. Faaij, L. Lundquist, U. Schenker, J.F. Briois, M.K. Patel, Life cycle impact assessment of bio-based plastics from sugarcane ethanol, J. Clean. Prod. 90 (2015) 114–127. https://doi.org/10.1016/j.jclepro.2014.11.071.

[41] M. Hasani, E.D. Cranston, G. Westman, D.G. Gray, Cationic surface functionalization of cellulose nanocrystals, Soft Matter. 4 (2008) 2238–2244. https://doi.org/10.1039/B806789A.

[42] H. Kangas, A. Suurnäkki, M. Kleen, Modification of the surface chemistry of TMP with enzymes, Nord. Pulp Pap. Res. J. 22 (2007) 415–423. https://doi.org/10.3183/npprj-2007-22-04-p415-423.

[43] H. Kangas, M. Kleen, Surface chemical and morphological properties of mechanical pulp fines, Nord. Pulp Paer Res. J. 22 (2004) 415–423.

[44] K. Sahlin, L. Forsgren, T. Moberg, D. Bernin, M. Rigdahl, G. Westman, Surface treatment of cellulose nanocrystals (CNC): effects on dispersion rheology, Cellulose. 25 (2018) 331–345. https://doi.org/10.1007/s10570-017-1582-5.

[45] S. Chattopadhyay, H. Keul, M. Moeller, Functional Polymers Bearing Reactive Azetidinium Groups: Synthesis and Characterization, Macromol. Chem. Phys. 213 (2012) 500–512. https://doi.org/10.1002/macp.201100480.

[46] V.V.R.M. Krishna Reddy, D. Udaykiran, U.S. Chintamani, E. Mahesh Reddy, C. Kameswararao, G. Madhusudhan, Development of an optimized process for the preparation of 1-benzylazetidin-3-ol: An industrially important intermediate for substituted azetidine, Org. Process Res. Dev. 15 (2011) 462–466. https://doi.org/10.1021/op100247m.

[47] P.G. Parzuchowski, A. Świderska, M. Roguszewska, T. Frączkowski, M. Tryznowski, Amine functionalized polyglycerols obtained by copolymerization of cyclic carbonate monomers, Polymer (Guildf). 151 (2018) 250–260. https://doi.org/10.1016/J.POLYMER.2018.07.055.

[48] X.M. Dong, J.F. Revol, D.G. Gray, Effect of microcrystallite preparation conditions on the formation of colloid crystals of cellulose, Cellulose. 5 (1998) 19–32. https://doi.org/10.1023/A:1009260511939.

[49] E.J. Foster, R.J. Moon, U.P. Agarwal, M.J. Bortner, J. Bras, S. Camarero-Espinosa, K.J. Chan, M.J.D. Clift, E.D. Cranston, S.J. Eichhorn, D.M. Fox, W.Y. Hamad, L. Heux, B. Jean, M. Korey, W. Nieh, K.J. Ong, M.S. Reid, S. Renneckar, R. Roberts, J.A. Shatkin, J. Simonsen, K. Stinson-Bagby, N. Wanasekara, J. Youngblood, Current characterization methods for cellulose nanomaterials, Chem. Soc. Rev. 47 (2018) 2609–2679. https://doi.org/10.1039/C6CS00895J.

[50] P.A. Larsson, A. V. Riazanova, G. Cinar Ciftci, R. Rojas, H.H. Øvrebø, L. Wågberg, L.A. Berglund, Towards optimised size distribution in commercial microfibrillated cellulose: a fractionation approach, Cellulose. 4 (2018) 1–11. https://doi.org/10.1007/s10570-018-2214-4.

[51] T. Moberg, K. Sahlin, K. Yao, S. Geng, G. Westman, Q. Zhou, K. Oksman, M. Rigdahl, Rheological properties of nanocellulose suspensions: effects of fibril/particle dimensions and surface characteristics, Cellulose. 24 (2017) 2499–2510. https://doi.org/10.1007/s10570-017-1283-0.

[52] A. Venkatesh, J. Thunberg, T. Moberg, M. Klingberg, L. Hammar, A. Peterson, C. Müller, A. Boldizar, Cellulose nanofibril-reinforced composites using aqueous dispersed ethylene-acrylic acid copolymer, Cellulose. 25 (2018) 4577–4589. https://doi.org/10.1007/s10570-018-1875-3.

[53] N.S. Allen, D. Lo, M. Sharif Salim, P. Jennings, Influence of amine structure on the post-cured photo-yellowing of novel amine diacrylate terminated ultraviolet and electron beam cured coatings, Polym. Degrad. Stab. 28 (1990) 105–114. https://doi.org/10.1016/0141-3910(90)90055-C.

[54] P. Xiao, S. Shi, J. Nie, Synthesis and characterization of copolymerizable one-component type II photoinitiator, Polym. Adv. Technol. 19 (2008) 1305–1310. https://doi.org/10.1002/pat.1132.

[55] W. Liu, C. Zhao, R. Zhou, D. Zhou, Z. Liu, X. Lu, Lignin-assisted exfoliation of molybdenum disulfide in aqueous media and its application in lithium ion batteries, Nanoscale. 7 (2015) 9919–9926. https://doi.org/10.1039/c5nr01891a.

[56] N. Wang, E. Ding, R. Cheng, Thermal degradation behaviors of spherical cellulose nanocrystals with sulfate groups, Polymer (Guildf). 48 (2007) 3486–3493. https://doi.org/10.1016/j.polymer.2007.03.062.

[57] F. Yao, Q. Wu, Y. Lei, Y. Xu, Rice straw fiber-reinforced high-density polyethylene composite: Effect of fiber type and loading, Ind. Crops Prod. 28 (2008) 63–72. https://doi.org/10.1016/j.indcrop.2008.01.007.

[58] T.H.S. Maia, N.M. Larocca, C.A.G. Beatrice, A.J. de Menezes, G. de Freitas Siqueira, L.A. Pessan, A. Dufresne, M.P. França, A. de Almeida Lucas, Polyethylene cellulose nanofibrils nanocomposites, Carbohydr. Polym. 173 (2017) 50–56. https://doi.org/10.1016/j.carbpol.2017.05.089.

[59] V. Khoshkava, M.R. Kamal, Effect of cellulose nanocrystals (CNC) particle morphology on dispersion and rheological and mechanical properties of polypropylene/CNC nanocomposites, ACS Appl. Mater. Interfaces. 6 (2014) 8146–8157. https://doi.org/10.1021/am500577e.

[60] D. Shumigin, E. Tarasova, A. Krumme, P. Meier, Rheological and Mechanical Properties of Poly (lactic) Acid / Cellulose and LDPE / Cellulose Composites, 17 (2011).

[61] Y. Chen, C. Xu, J. Huang, D. Wu, Q. Lv, Rheological properties of nanocrystalline cellulose suspensions, Carbohydr. Polym. 157 (2017) 303–310. https://doi.org/10.1016/j.carbpol.2016.10.002.

[62] A.K. Townsend, H.J. Wilson, Small- and large-amplitude oscillatory rheometry with bead–spring dumbbells in Stokesian Dynamics to mimic viscoelasticity, J. Nonnewton. Fluid Mech. 261 (2018) 136–152. https://doi.org/10.1016/J.JNNFM.2018.08.010.

[63] R. Guo, J. Azaiez, C. Bellehumeur, Rheology of fiber filled polymer melts: Role of fiber-fiber interactions and polymer-fiber coupling, Polym. Eng. Sci. 45 (2005) 385–399. https://doi.org/10.1002/pen.20285.

[64] M. Hietala, K. Oksman, Pelletized cellulose fibres used in twin-screw extrusion for biocomposite manufacturing: Fibre breakage and dispersion, Compos. Part A Appl. Sci.

Manuf. 109 (2018) 538–545. https://doi.org/10.1016/j.compositesa.2018.04.006.

[65] K.B. Adhikary, C.B. Park, M.R. Islam, G.M. Rizvi, Effects of Lubricant Content on Extrusion Processing and Mechanical Properties of Wood Flour-High-density Polyethylene Composites, J. Thermoplast. Compos. Mater. 24 (2011) 155–171. https://doi.org/10.1177/0892705710388590.

[66] J. Kubát, M. Rigdahl, M. Welander, Characterization of interfacial interactions in high density polyethylene filled with glass spheres using dynamic-mechanical analysis, J. Appl. Polym. Sci. 39 (1990) 1527–1539. https://doi.org/10.1002/app.1990.070390711.

[67] L.E. Nielsen, Mechanical properties of polymers and composites - Vol.2, M. Dekker, 1994.

Errata List for the Doctoral defence

Abhijit Venkatesh

January 22, 2021

This document lists the errors found in the printed version of Abhijit Venkatesh's doctoral thesis 'Melt-processing and properties of thermoplastic composites based on ethylene-acrylic acid reinforced with wood nanocellulose', with corrections where applicable.

Location	Original text	Correction
Page 23, Line 10	As expected, the highly beaten never-dried pulp fiber (reference pulp in Paper I) had higher fines content and smaller dimensions than the TMP based fiber.	**The TMP fibers had higher fines content than the highly beaten never-dried pulp fibers (reference pulp in Paper I).**
Page 23, Table 3	Length (nm) Width (nm) CNC (Paper II) – 6 ± 1.5 211 ± 114 CNC (Paper III) – 6 ± 3 301 ± 110	Length (nm) Width (nm) CNC (Paper II) – **211 ± 114** **6 ± 1.5** CNC (Paper III) – **301 ± 110** **6 ± 3**
Page 28, Line 16	The S1 screw configuration ……size of the aggregates with increasing number of passes, see Figure 13 (a), (b) and (c).	The **combination of** S1 screw configuration ……size of the aggregates with increasing number of passes, **see Figure 13(a).**
Page 31, Line 19	Figure 18 shows the 10 wt% CNC composites placed on the Kofler bench at 120, 130, 10,150 and 160 °C.	Figure 18 shows the 10 wt% CNC composites placed on the Kofler bench at 120, 130, **140**, 150 and 160 °C.
Page 40, Table 6	(No yield stress values were given for EAA7-10% CNC and EAA7-10% diallylCNC samples produced from Celluforce CNC via compression moulding - produced as Reference.)	*Yield Stress (MPa)* EAA7-10% CNC – **16.3 (0.2)** EAA7-10% CNC – **15.4 (0.1)**
Paper I, Figure 2, Legend	—— 1.8 wt.% CNF /0.49 wt.% EAA/ 97.7 wt.% water - - - 0.7 wt.% CNF /3.96 wt.% EAA/ 95.3 wt.% water	- - - 1.8 wt.% CNF /0.49 wt.% EAA/ 97.7 wt.% water —— 0.7 wt.% CNF /3.96 wt.% EAA/ 95.3 wt.% water

Paper I, Page 4581, Col 2, Line 23	Interestingly, the CNF content in the suspensions did not appear to affect the slope in the region of shear thinning.	Interestingly, the CNF content in the suspensions did not appear to affect the slope **in the non-linear region.**
Paper I, Page 4581, Col 1, Equation 3	$E_{f,l} = \frac{3/8(Ec - 5/8ET) - Em(1-\Phi)}{\Phi}$	$E_{f,l} = \frac{\mathbf{8/3}(Ec - 5/8ET) - Em(1-\Phi)}{\Phi}$
Paper III, Fig 12, Legend	**Figure 12:** The viscosity (η) and loss moduli ($\dot{\gamma}$) for **(a)** CNF- *(symbols)* and CNC- *(lines)* containing composites compounded using S1 *(solid symbols)* or S2……**(b)** CNF-containing composites compounded with S1 screw configuration and shaped using either the Maddock type *(solid symbols)* or the Maillefer barrier screw *(open symbols)*	**Figure 12:** The **viscosity and shear rate** for **(a)** CNF- *(symbols)* and CNC- *(lines)* containing composites compounded using S1 *(solid symbols)* or S2…….**(b)** CNF-containing composites compounded with S1 screw configuration and shaped using either the Maddock type ***(open symbols)*** or the Maillefer barrier screw ***(solid symbols)***
Paper III, Fig 12, Inset plot	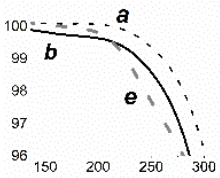	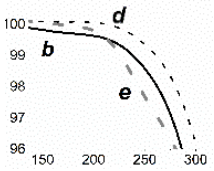
Paper IV, Fig 1, Caption	Mechanical loss factor as a function of….30 wt% (open squares), 50 wt% (open circles) and 70 wt% (open triangles) (a) TMP and (b) DP	Mechanical loss factor as a function of….**30 wt%, 50 wt% and 70 wt%** (a) TMP and (b) DP